Politecnico di Torino

Politecnico di Torino

Master's Degree in Mechatronic Engineering

A.y 2024/2025

December graduation session 2024

Structural optimisation of Tension Leg Platform for an Offshore Wind Turbine

Supervisor:
Giovanni BRACCO

Advisor:
Massimo SIRIGU

Candidate:
Dilshodbek Abduvaitov

ABSTRACT

Wind power has already proved to be a sustainable energy resource capable of providing the world with fossil fuel-free energy. Offshore Wind Turbines (OWTs) have emerged as one of the most efficient implementations of wind energy since they can utilize the most persistent wind resources available offshore and have much higher efficiencies than onshore wind turbines. The rapid global deployment of Offshore Wind Farms, specifically Floating Offshore Wind Turbines (FOWTs), has been enabled by recent technological advancements that allow FOWTs to be deployed further offshore in deeper waters where traditional fixed-bottom structures cannot. Despite this, unique challenges exist in the design and deployment of FOWTs with respect to structural performance, cost-effectiveness, and sustainability. Developing floating platforms that are both reliable and long-lasting while still standing up to harsh marine conditions presents considerable technical as well as economic challenges for engineers. One of the most common types of Floating Offshore Wind Turbines is the high stability Tension Leg Platform (TLP), which uses a tensioned mooring

system. This thesis will be dedicated to the parametric analysis and structural optimization of Tension Leg Platform types. This work aims to conduct a parametric structural optimization of the TLP platform using Finite Element Methods. The initial analysis consists of hydrodynamic and aerodynamic loads, static and dynamic forces, and interaction between the turbine and mooring system. OpenFAST software is used to simulate the complex static and dynamic characteristics of the wind turbine, including governing tower loads and force distribution on mooring lines. In order to provide for a realistic and conservative design of the platform, this thesis also encompasses hydrostatic pressure, turbine weight, static aerodynamic thrust, and mooring loads into the structural analysis. Central to this work is the application of a single-objective optimization algorithm designed to minimize platform mass subject to mechanical stress and buckling instability constraints. The location and setting of internal stiffeners inside the platform are given special attention to improve structural performance. The findings in this work indicate that, with a fine-tuned selection of stiffener locations, the global mass of the platform can

be drastically reduced while still achieving structural performance under operational structural loads. In addition, the trade-off between platform geometry and load distribution, together with implications on material usage, are discussed to provide insights for improving future designs and further reducing FOWT development costs.

Contents

List of Figures

List of Tables

Chapter 1

INTRODUCTION

The wind has emerged as an important source of the world's energy, marking one of the monumental events of the 20th century. While industrial advancement completely depended on fossil fuels, an awareness of the finiteness of the Earth's fossil fuel reserves, as well as the detrimental impacts of burning these fuels for energy, has led engineers in search of alternatives and renewable sources of energy. In addition to this high density, at the very least in parts of the world, wind power has been abundant, promoting research for its conversion technology and harvesting electricity from wind power. While the reasons mentioned above seemed to have set the stage for a technological revolution in the energy sector, these were not enough to trigger the revival of wind power until technological capacity and political reforms created space for a new technology — wind turbines. Put differently, the scale of the structure and other costs could not have expanded to this extent without government funding. Finally, the required political will for this support emerged

at different times and to varying degrees in many nations: first Washington, Copenhagen, and Berlin; now across most of the planet.

Many onshore and offshore installations using this technology are now made possible with recent advances in technology. It is expected that offshore wind turbines will outweigh onshore wind turbines in spite of their relatively lower capital cost and simple construction. First of all, the power density of offshore wind is higher than that of onshore wind, and so is the energy production. Regarding environmental impacts, onshore wind farms can disrupt habitats, cause noise pollution, affect native species, as well as result in visual impairment for nearby residents; but these effects are generally lower than those seen associated with other types of energy production systems, such as fossil fuels. Last but not least, land use can lead to negative consequences because land shortage is important today due to population growth. However, the high capital investment, installation, and maintenance costs may offset some of the benefits of offshore wind turbines. Thus, a lot of research and development is being carried out around the world to bring down these costs.

The aim of this thesis is to study the Floating Offshore Wind Turbine of Tension Leg Platform type and develop the optimal structural design of the platform by utilizing the Finite Element method. Initially, the load transferred to the tower and mooring lines is calculated using static and dynamic analysis approaches in OpenFAST software. Structural analysis is performed considering hydrostatic pressure, static aerodynamic thrust, turbine weight, and mooring loads. Final consideration is given to a single-objective optimization algorithm aimed at minimizing mass and constraining mechanical stress and buckling instability. It reveals that both the type and position of the internal stiffeners are fundamental in order to minimize global mass and reduce mechanical stress.

Chapter 2

LITERATURE REVIEW

2.1 Electricity Production

In contemporary society, electricity serves as a crucial resource, integral to various daily activities ranging from professional tasks to leisure. The demand for electricity is rising significantly, driven by factors such as the shift towards electric transportation, the proliferation of connected devices, and the ongoing digital transformation of modern economies [1].

Electricity production is categorized in many different ways, each with its own features, advantages, and disadvantages. Traditional fossil fuel power generation — coal, oil, and gas — consists of burning these fuels to generate steam from heated water that turns turbines to generate power.

Coal is a non-renewable fossil fuel, and while it serves as an energy source, its significant drawback lies in its environmental consequences. Although this technique is

unsustainable and provides minimal upfront costs, it represents a substantial portion of greenhouse gas emissions, air pollution, and ecological degradation. The burning of coal releases various pollutants into the atmosphere, including sulfur dioxide (SO2), carbon dioxide (CO2), nitrogen oxides (NOx), and particulate matter [2]. Figure 1 describes the electricity production from fossil fuels.

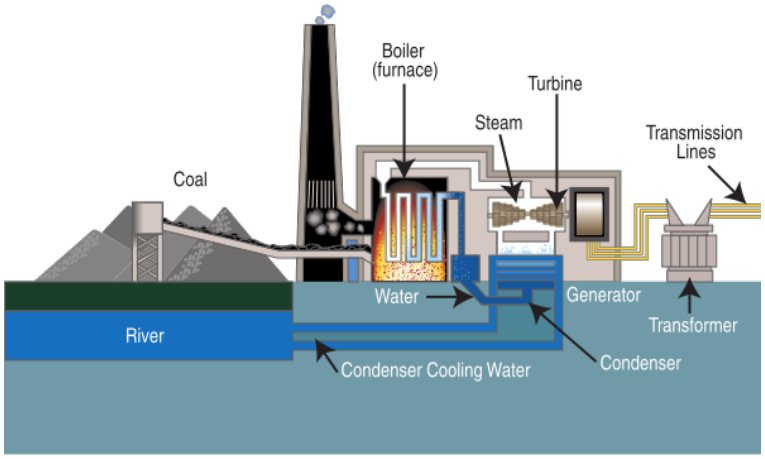

Figure 1: Electricity production from Fossil fuels [4].

Nuclear power has low greenhouse gas emissions, using nuclear fission reactions to heat water and support turbines generating electricity, but it comes with very high upfront construction costs and concerns about both catastrophic accidents and nuclear waste that has long half-lives. Nuclear power is an important low-emission source of electricity, providing about 10% of global elec-

tricity generation [3]. Figure 2 depicts the diagram of Nuclear plant.

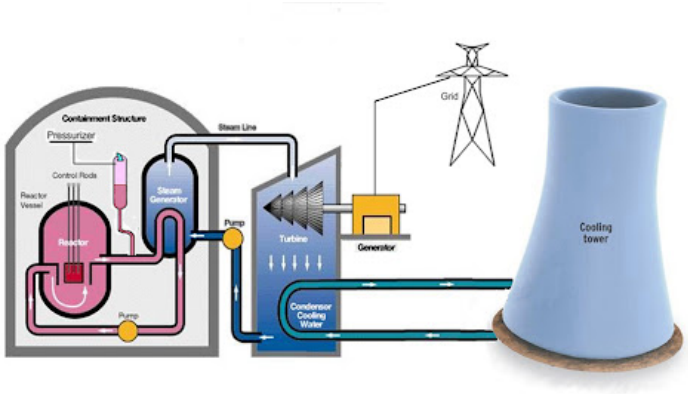

Figure 2: Nuclear power-based energy generation [63].

2.2 Renewable sources of energy

On the other hand, renewable energy sources like hydropower, wind power, solar power, biomass energy, and geothermal energy provide a more sustainable and environmentally friendly alternative. From hydroelectric dams that capture the kinetic energy of flowing water and convert it through turbines into usable electricity, offering added benefits like flood control and irrigation.The amount of precipitation that drains into rivers and streams in a geographic area determines the amount of water avail-

able for producing hydropower [5]. Hydroelectric dam structure is illustrated in figure 3.

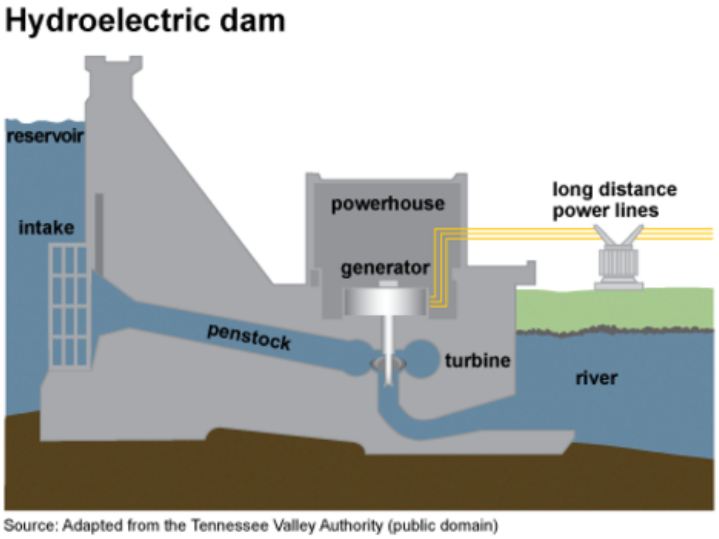

Figure 3: Hydroelectric dam architecture [64].

Solar energy, using photovoltaic panels to directly convert sunlight into electricity, is abundant, modular, and scalable, though also periodic and expensive at first. When sunlight strikes a solar panel, the photovoltaic (PV) cells within it capture energy from the light. This absorbed energy generates electrical charges that respond to an internal electric field present in the cell, resulting in the generation of electricity [7]. Electricity production from solar energy is shown in figure 4.

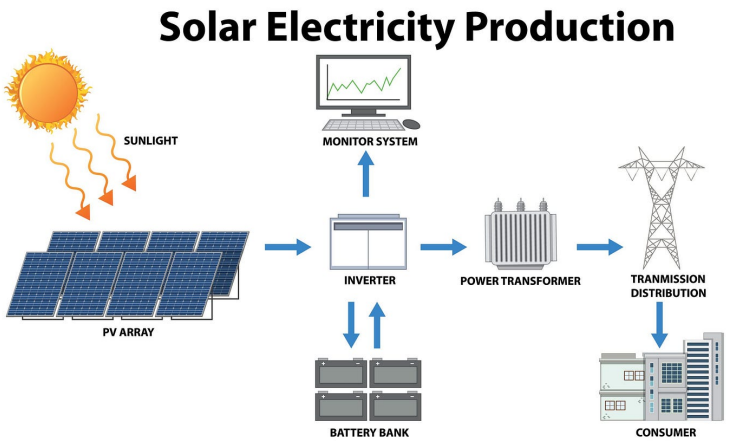

Figure 4: Electricity generation from solar energy source [6].

Biomass is renewable organic material that comes from plants and animals [8]. Biomass energy is obtained from burning organic molecules to heat water and create steam that drives an electricity generator, which can be sustainable if the biomass is sourced sustainably but creates greenhouse emissions and air pollution. Biomass served as the predominant source of total annual energy consumption in the United States until approximately the mid-1800s. As of 2023, it represented around 5% of the nation's overall primary energy usage [8]. This resource is utilized for generating electricity and heat, as well as a fuel for transportation. Biomass remains a crucial energy source in various countries, particularly in developing nations, where it is widely used for cooking and heating

purposes.

Geothermal energy is the clean and renewable energy from heat generated in the Earth, which can be harnessed as steam to deliver electricity [9]; however, it is limited by certain geological constraints and beset with high development costs. Figure 5 presents electricity production process from geothermal energy.

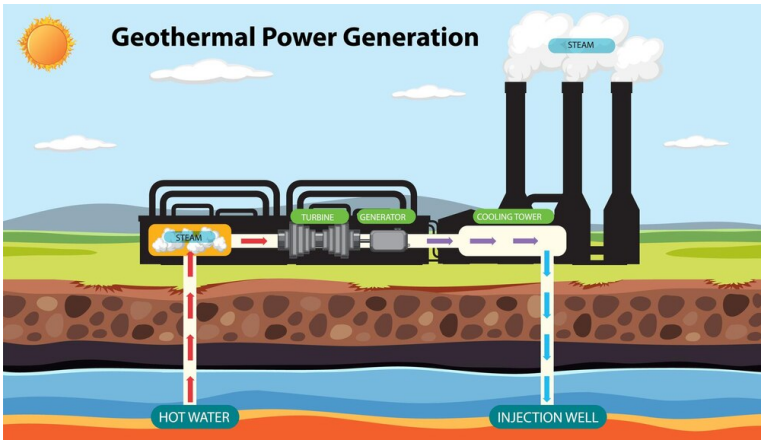

Figure 5: Electricity generation from geothermal energy [10].

Wind energy transforms the kinetic energy of wind into electricity through turbines, guaranteeing quick and easy scaling; however, it is intermittent and poses a threat to wildlife. A wind turbine turns wind energy into electricity using the aerodynamic force from the rotor blades, which work like an airplane wing or helicopter rotor blade.

When wind flows across the blade, the air pressure on one side of the blade decreases. The difference in air pressure across the two sides of the blade creates both lift and drag [11]. The lift generated is greater than the drag, resulting in the rotor's rotation. This rotor is linked to the generator, which can be done directly in a direct drive turbine or via a shaft and a series of gears (gearbox) that enhance the rotational speed, enabling a more compact generator design. This conversion of aerodynamic force into generator rotation produces electricity. The wind turbines that transfer electricity to the grid are either based on land (onshore) or at sea (offshore). Conglomerations of wind turbines are known as wind farms [14].

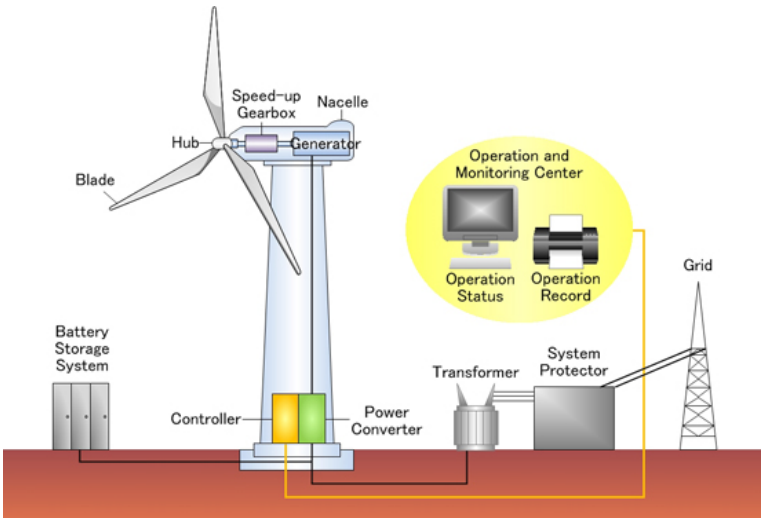

Figure 6: Electricity generation from Wind Energy [65].

Renewable energy has many well-known drawbacks; they cannot always produce power (intermittency), they have a ceiling applied to drive them from windy or sunny areas (geographic limitations), and the installations will inevitably disturb the environment (environmental impacts). For instance, during rainy weather, photovoltaic panels are unable to produce electricity, necessitating a return to conventional power sources [12]. This unpredictability is a significant disadvantage of depending on renewable technologies.

Each energy type necessitates particular technologies to transform it into electricity. When assessing energy sources, the efficiency of these conversion devices plays a crucial role. Regrettably, the efficiency of renewable energy technologies tends to be lower in comparison to conventional energy conversion systems. For instance, commercially available solar panels have an efficiency range of 15% to 20%. In contrast, traditional technologies that utilize coal or natural gas can achieve efficiency rates as high as 40% and 60%, respectively [12].

Considering the energy potential of renewable technologies, their upfront expenses can be substantial and occa-

sionally prohibitive [12]. The production and installation of renewable energy systems, such as photovoltaic panels, tend to incur significant costs. Additionally, heat pumps may be quite expensive for certain households. In response, governments are allocating substantial funds, including grants for solar panels and heat pumps, to promote the development of these technologies.

To effectively utilize the energies provided by nature, a significant amount of space is required. This necessity presents various challenges for sites dedicated to renewable energy. In contrast to conventional power plants, renewable energy farms demand a larger land area for their establishment [12].

However, these technologies are rapidly maturing and becoming more affordable; their contribution to the global electricity mix is growing more significant year by year. Decarbonizing energy systems is fueled by climate change mitigation, the finite nature of fossil fuel resources, and a green promotion of (sustainable) energy utilization security and independence. With continual advancements in renewable energy technologies, they present a promising solution to achieve a clean, sustainably connected electric-

ity production system. However, these technologies are rapidly maturing and becoming more affordable; their contribution to the global electricity mix is growing more significant year by year. Decarbonizing energy systems is fueled by climate change mitigation, the finite nature of fossil fuel resources, and a green promotion of (sustainable) energy utilization security and independence. With continual advancements in renewable energy technologies, they present a promising solution to achieve a clean, sustainably connected electricity production system. Fig. 7 illustrates the overall usage of renewable energy for electricity generation from 2010 to 2020 [13]. The International Energy Agency's global energy review in 2021 indicates that total renewable energy consumption rose significantly, increasing from 4,098 TWh in 2010 to 7,627 TWh in 2020. Hydropower remains the largest contributor to global renewable energy capacity for electricity production, despite its slower growth rate relative to other renewable sources.

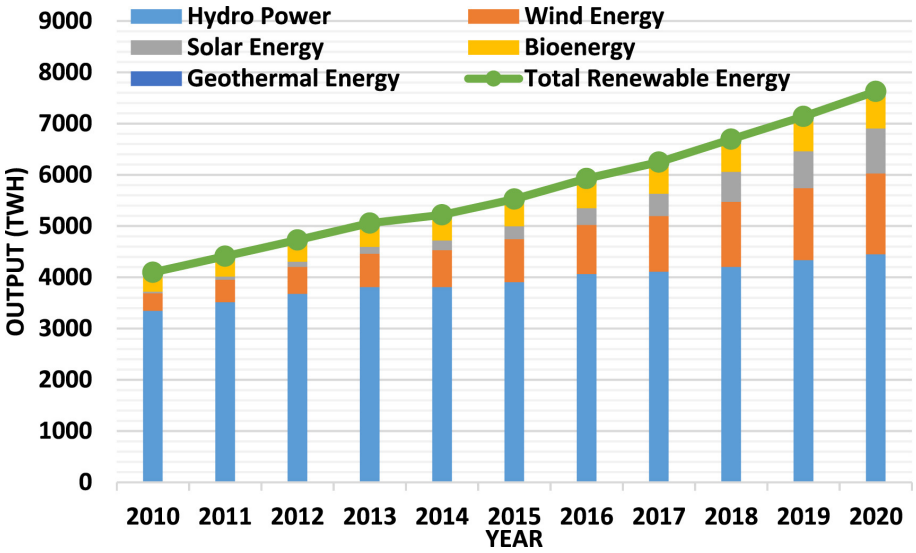

Figure 7: Comparison of renewable energies [13].

In contrast, solar energy generation is on the rise, driven by ongoing advancements and improvements in solar technologies aimed at enhancing energy conversion efficiency. Wind energy generation also demonstrates a notable upward trend. Conversely, bioenergy and geothermal energy have had minimal contributions since 2010 due to the limited geographical suitability for geothermal power plants and the complexities involved in bioenergy production.

2.3 Wind power potential

Wind power is emerging as a prominent renewable energy source with vast potential for electricity generation. Harnessing the kinetic energy of wind through the use of turbines, wind power offers several advantages, including rapid deployment, scalability, and relatively low environmental impact. As technology has advanced, wind turbines have become more efficient and cost-effective, driving down the overall cost of wind power generation. Between 2010 and 2020, the global weighted-average levelised cost of electricity (LCOE) of onshore wind fell by 56%, from USD 0.089/kWh to USD 0.039/kWh. Over the same period, the LCOE of newly commissioned offshore wind projects fell by around half (48%) [15]. Wind turbine capacity has increased over time. In 1985, typical turbines had a rated capacity of 0.05 MW and a rotor diameter of 15 metres. Today's new wind power projects have a turbine capacity in the 3-4 MW range onshore and 8-12 MW offshore [15]. Additionally, wind power is a domestic resource, reducing dependence on imported fuels and promoting energy security. Geographically, wind power can be particularly advantageous in areas

with high wind power density, such as coastal regions, plains, and mountain passes. These areas offer consistent and strong wind patterns, maximizing energy output. The amount of power that can be harvested from wind depends on the size of the turbine and the length of its blades. The output is proportional to the dimensions of the rotor and to the cube of the wind speed. Theoretically, when wind speed doubles, the wind power potential increases by a factor of eight [15]. While wind power does have limitations, such as intermittency and visual and noise impacts, technological advancements, along with improvements in energy storage and grid integration, are addressing these challenges. As a result, wind power is playing an increasingly significant role in the global energy transition, providing a clean, renewable, and sustainable source of electricity. The bar chart in figure 8 illustrates the worldwide increase in electricity generation capacity from both onshore and offshore wind energy from 2012 to 2023, measured in megawatts (MW). Throughout this time frame, there is a notable upward trend in the overall capacity for wind energy, indicating a growing reliance on wind power as a feasible sustainable

energy option.

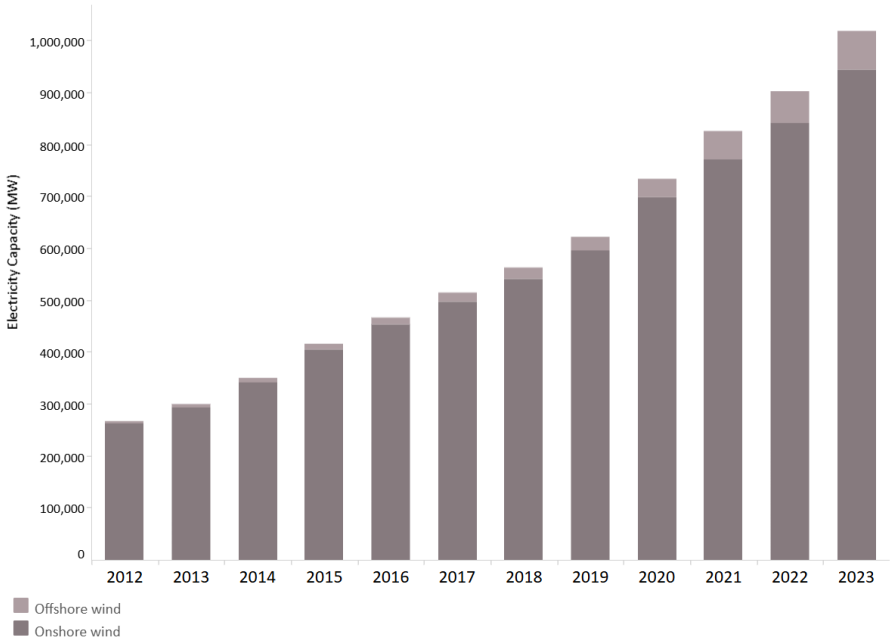

Figure 8: Comparison of electricity capacities of onshore and offshore wind [15].

Onshore wind energy consistently accounts for the bulk of this capacity, whereas offshore wind, despite accounting for a smaller portion, shows consistent growth. The total capacity peaks in 2023 reflect ongoing advancements and investments in wind energy infrastructure. This information underscores the essential role that wind energy plays in the shift towards renewable energy systems and in meeting global sustainability objectives.

2.4 Wind turbines

Wind turbines are complex machines designed to convert the kinetic energy of wind into electrical energy. Wind turbines fall into two basic categories: horizontal-axis turbine and vertical-axis turbine. HAWTs, characterized by a horizontally aligned rotor shaft and blades, are highly efficient and dominate large-scale wind energy production, both onshore and offshore [16]. These turbines require yaw mechanisms to face the wind and are well-suited for locations with consistent wind patterns. In contrast, VAWTs have a vertical rotor shaft, allowing them to operate independently of wind direction [17], making them ideal for urban or small-scale settings with turbulent or variable winds. While VAWTs are simpler in design, easier to maintain, and suitable for localized applications, they are generally less efficient and produce lower energy output compared to HAWTs [18]. Together, these technologies offer complementary solutions for maximizing wind energy utilization across different environments. Figure 9 depicts the comparison between HAWT and VAWT.

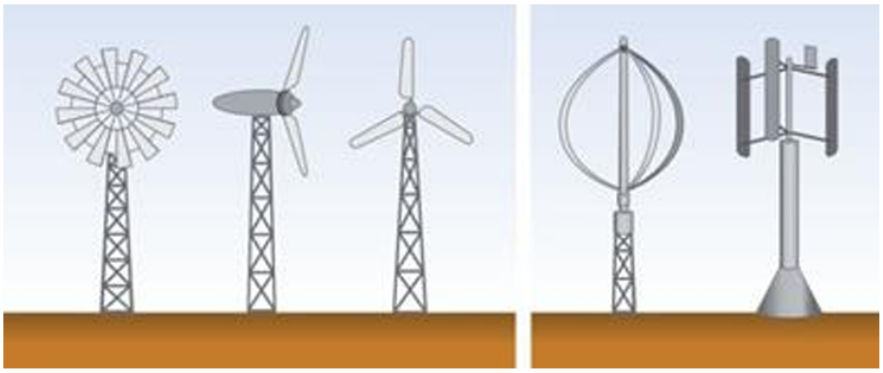

Figure 9: Horizontal-Axis Turbines on the left and Vertical-Axis Turbines on the right [20].

Wind Turbines can also be classified according to the direction of wind.

- **Upwind:** In this configuration, the wind first interacts with the blades before passing through the tower, which minimizes shadowing effects. This arrangement promotes smoother operation and enhances power generation. It is the predominant design and is illustrated in Figure 10 on the left.
- **Downwind:** Conversely, in this setup, the wind flows past the tower prior to reaching the blades. This sequence leads to significant shadowing effects that can induce flexural stress on the blades, resulting in increased fatigue for the overall structure due to a rise in flexion cycles [21]. A downwind turbine is

depicted in Figure 10 on the right.

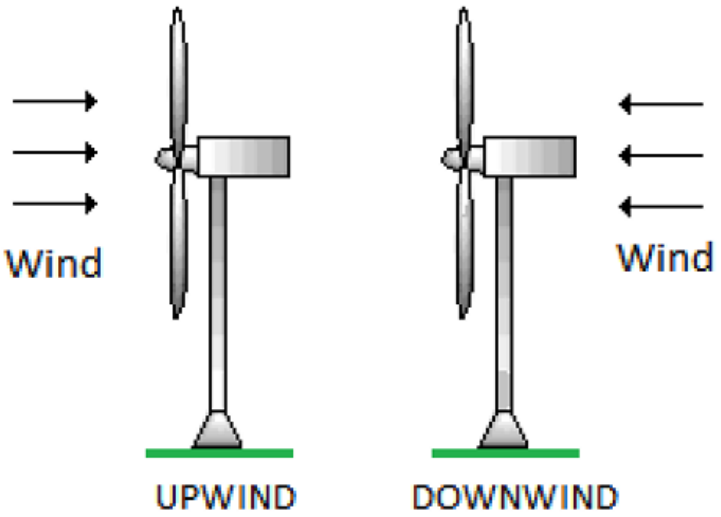

Figure 10: Distinction between Upwind and Downwind Wind Turbines [21].

A typical wind turbine consists of several key components, each playing a crucial role in the generation process, some of which are depicted in figure 11.

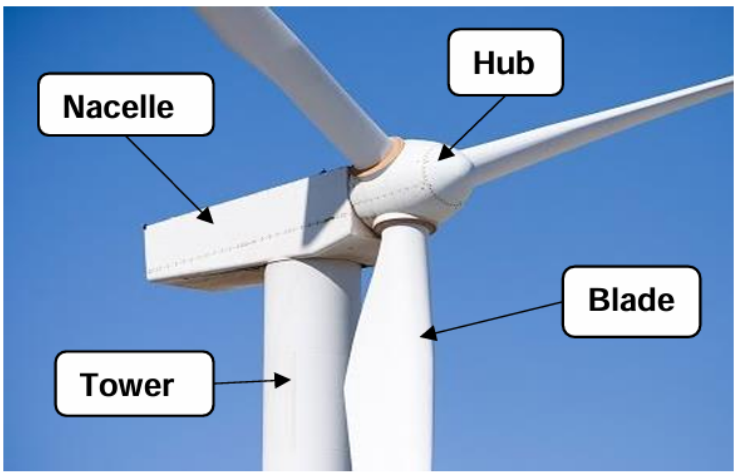

Figure 11: Wind turbine [66].

1. **Rotor Blades:** The rotor blades capture the energy from the wind and convert it into rotational energy.

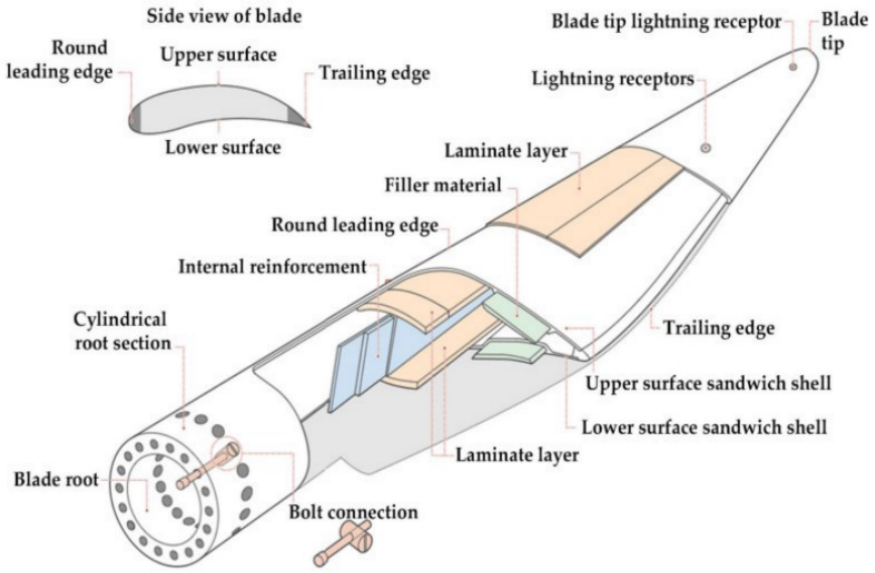

Figure 12: Rotor blade architecture [67].

Typically made from fiberglass or carbon-reinforced plastic, these blades are aerodynamically designed to maximize energy capture [19]. Modern wind turbines can have rotor blades ranging from 40 to 90 meters (130 to 295 feet) in length. A typical blade architecture is displayed in figure 12.

There are various designs that incorporate different quantities of blades per turbine. Figure 13 illustrates both a two-bladed turbine and a one-bladed turbine

design. The choice to utilize three blades is essentially a compromise; as the blades move through the air, they generate turbulence that influences the airflow directed towards the subsequent blade. An increase in blade count results in more chaotic airflow impacting the next blade. Consequently, theoretically, having only one blade would be optimal. However, this design poses significant drawbacks, including potential imbalance and instability of the turbine due to its singular blade configuration [22,23]. Thus, opting for two blades appears to be a more suitable alternative. While this option may offer cost benefits, it tends to be slightly less efficient than three-bladed models since it requires higher rotational speeds to achieve equivalent energy output [24]. Additionally, ensuring proper yaw alignment becomes quite challenging; when positioned horizontally, substantial forces are needed to align the rotor, whereas minimal forces are necessary when the blades are vertical. This situation leads to cyclic forces that exceed those experienced by three-bladed turbines [25,26]. Ultimately, employing three blades serves as an ideal solution, providing

enhanced stability, increased longevity, and superior energy production [23].

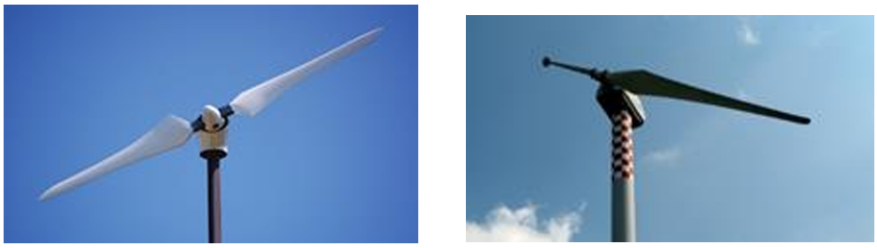

Figure 13: Two bladed turbine on the left [25]; one bladed turbine on the right [22].

2. **Hub:** The hub is the central component to which the rotor blades are attached. It sits atop the tower and houses the machinery that drives the generator. The hub's main function is to transfer the rotational energy from the blades to the generator. Figure 14 illustrates hub architecture.

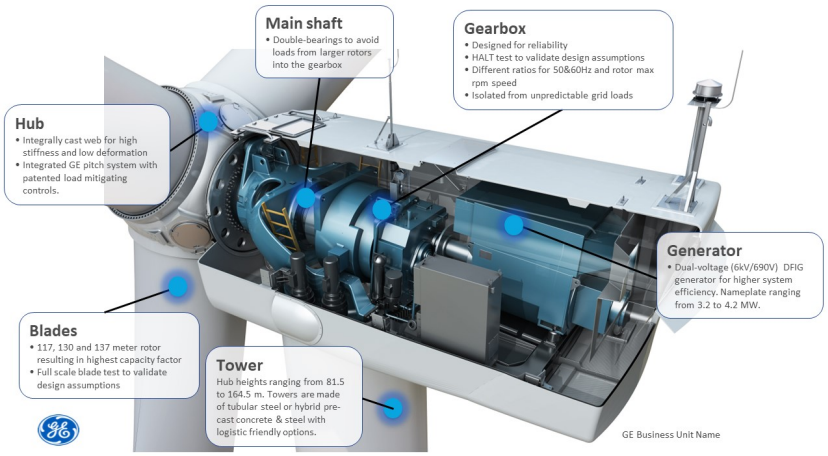

Figure 14: Hub architecture [68].

3. **Nacelle:** The nacelle is a large, enclosed structure that sits behind the rotor hub and comprises of the turbine's main mechanical and electrical components such as the gearbox, generator, controller, and other electronic systems. The nacelle is usually mounted on top of a tall tower to capture stronger and more consistent winds.

4. **Gearbox:** In many turbines, the rotational speed of the blades is not suitable for directly driving the generator. The gearbox increases the rotational speed to a level appropriate for the generator. It also allows the turbine to generate electricity even at low wind speeds. Figure 15 describes wind turbine gearbox.

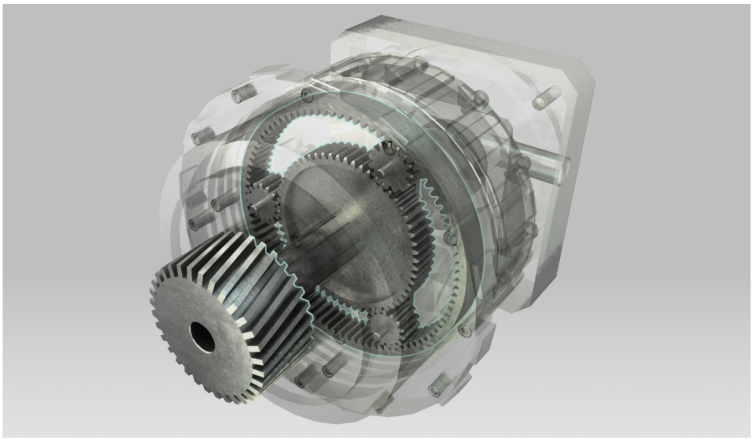

Figure 15: Wind Turbine Gearbox [27].

5. **Generator:** The generator is responsible for convert-

ing the mechanical energy from the rotating shaft into electrical energy. Most modern wind turbines use a type of generator known as a "synchronous generator" or "asynchronous induction generator." These generators produce alternating current (AC), which is then converted to the appropriate voltage for transmission to the grid. Some generators are driven by gearboxes and others are direct-drives where the rotor attaches directly to the generator [28].

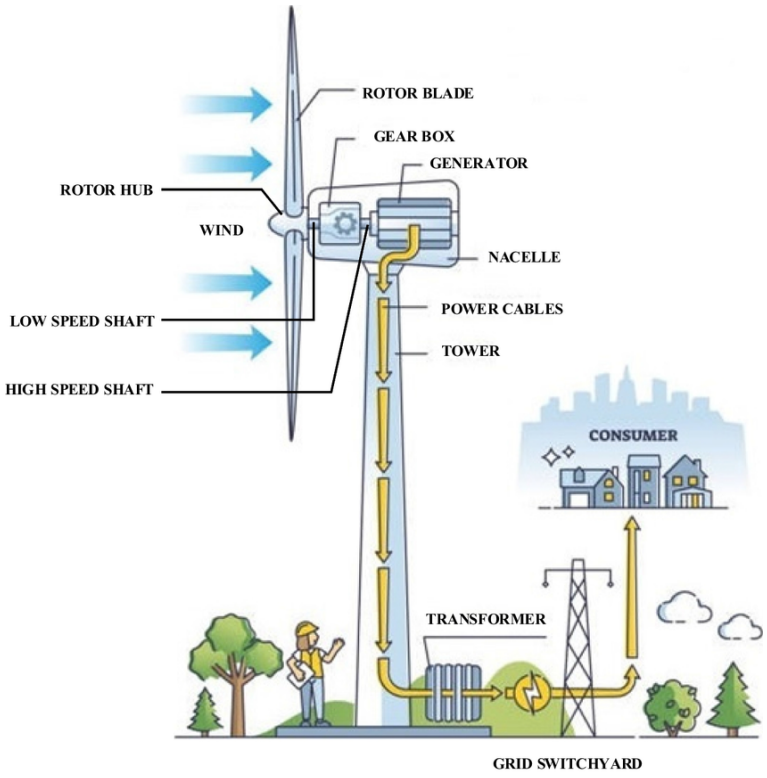

Figure 16: Wind Turbine Generator [69].

6. **Yaw System:** As the wind shifts, the turbine adjusts

its orientation to optimize energy generation under varying conditions. The yaw system is responsible for turning the nacelle and rotor blades to face into the wind. This ensures that the turbine captures the maximum amount of wind energy available. The yaw system is controlled by a weather vane or wind sensor, which continuously monitors wind direction. Yaw system is described in figure 17.

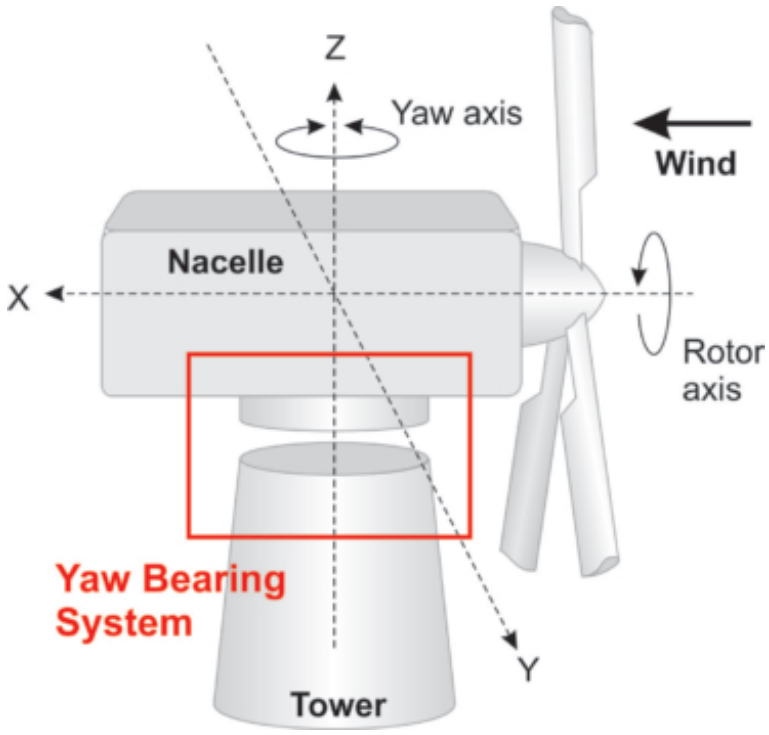

Figure 17: Wind Turbine Yaw system [70].

7. **Tower:** The tower provides the necessary height to elevate the rotor blades into the stronger and more

consistent winds present at higher altitudes. Towers can vary in height depending on the turbine's design and location, with typical heights ranging from 60 to 120 meters (200 to 400 feet), as depictes in figure 18.

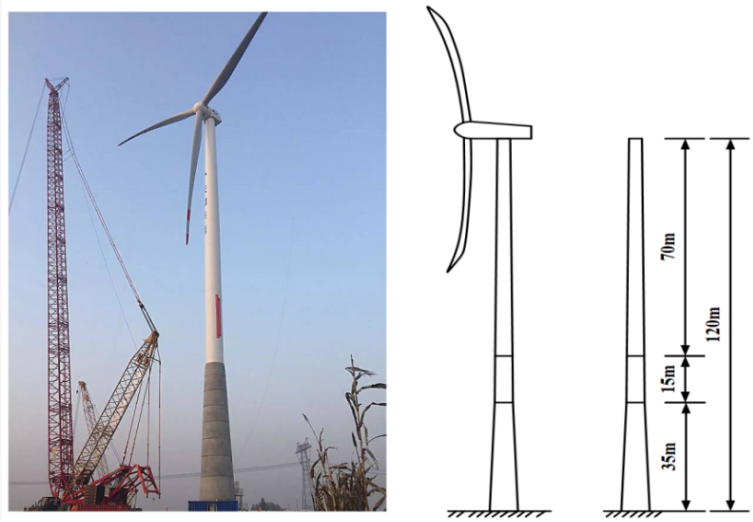

Figure 18: Wind Turbine Tower [71].

2.5 Offshore foundations

The primary obstacle facing offshore wind energy development lies in creating a cost-effective and appropriate platform for the turbines [28]. This platform serves as the foundational structure that must be constructed to support both the turbine and its associated loads. A

crucial determinant in the design and manufacturing of these structures is the depth of the sea at the installation site.

The depth of the sea at the continental shelf is typically categorized into three distinct classifications:

- **Shallow water:** up to 30 meters.
- **Transitional water:** from 30 to 60 meters.
- **Deep water:** deeper than 60 meters [20].

Foundations can be primarily classified into two main types according to the depth of the sea at the installation location [20]:

- **Bottom-fixed foundations:** foundations that are directly fixed to the sea floor. The most common examples are:
  - Monopile.
  - Jacket.
  - Gravity based foundation.
  - Tripod [20].
- **Floating foundations:** floating platform connected

to the sea floor through mooring lines. The most common examples are:

  – Spar-Buoy.

  – Semi-Submersible.

  – Tension Leg Platform (TLP) [20].

2.5.1 Bottom Fixed foundations

The predominant solutions utilized are those with fixed foundations at the bottom. These options can remain economically feasible for depths of up to 60 meters, contingent upon the structural type [29]. An overview of the key design variations will be provided.

- **Monopile Foundation:** it represents the most common type of foundations used for Offshore Wind Turbines. It consists of a steel pile of diameter between 2.5 and 6 meters [32], directly driven to the seabed in a total length from 10 to 20 meters. Although this type of foundation is primarily used in shallow water depths, they represent, as of 2023, around 80% of installed capacity [30]. Figure 19 illustrates the

structure of Monopile foundation.

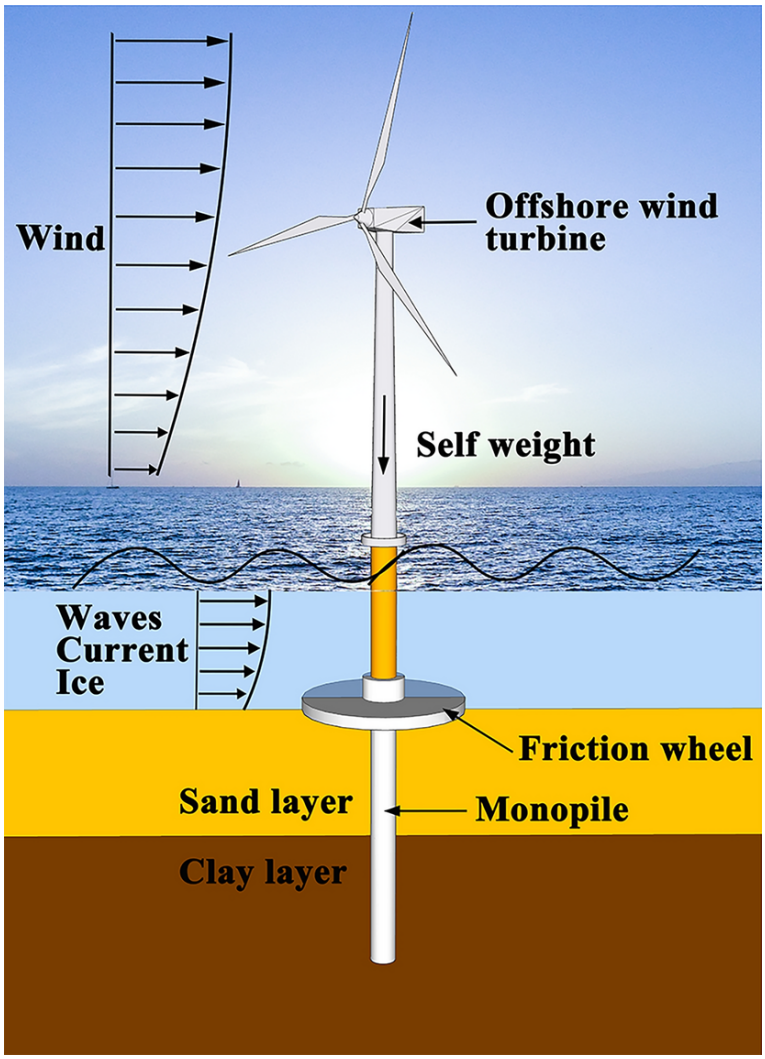

Figure 19: Monopile foundation [31].

- **Jacket Foundation:** The jacket foundation consists of a space frame structure constructed from steel tubes, depicted in figure 20, typically manufactured on land through welding processes prior to installation. Once completed, the jacket is then transported to the seabed

for piling. While jacket foundations are generally cost-effective regarding steel usage, they may incur significant expenses related to storage, logistics, and installation [33]. In recent years, jacket foundations have been used extensively in intermediate depths between 5 and 50 meters.

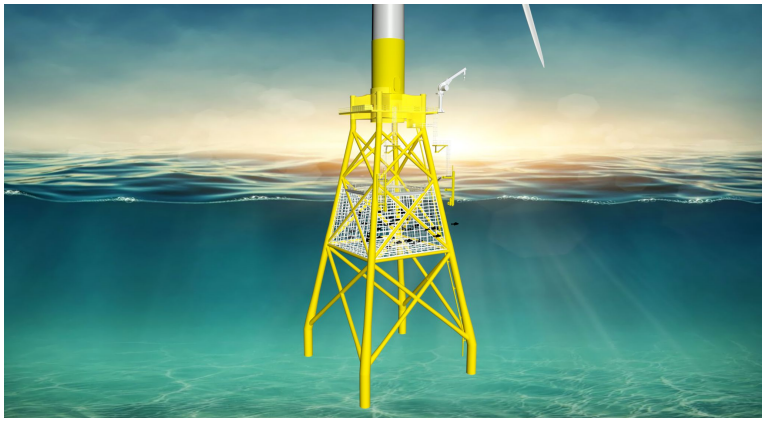

Figure 20: Jacket foundation [35].

- **Gravity Based Foundation:** This structure typically consists of a concrete framework featuring a central steel shaft that serves as the connection to the turbine tower, described in figure 21. The predominance of concrete in its construction enhances its durability in marine environments and minimizes maintenance requirements. A flat seabed is essential for this structure, necessitating prior preparation. One significant benefit of this design is the "float and submerge"

principle. This allows the structure to float on water, enabling tugboats to transport it rather than relying on large transport vessels, thereby reducing both transportation and installation expenses. The second aspect of this method, "submerge," involves positioning the foundation at the installation site where it can be lowered into place. This is accomplished by introducing water as ballast into the foundation to sink it onto the prepared seabed. Once accurately positioned, the water ballast is generally replaced with sand, which ensures stability for the structure [34].

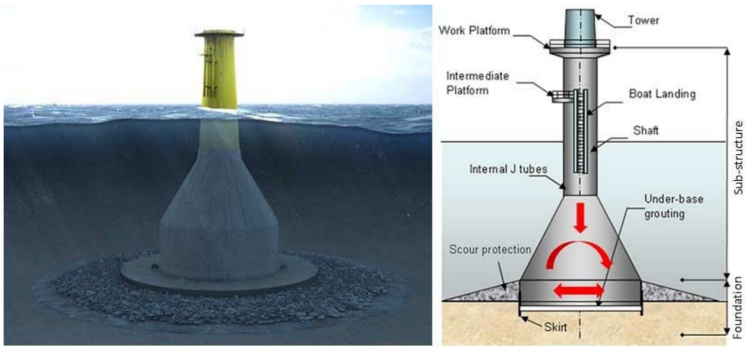

Figure 21: Gravity Based Foundation (illustration: Universal foundations).

- **Tripod Foundation:** The tripod consists of a three-legged framework constructed from cylindrical steel tubes. Its central steel shaft connects to the wind tur-

bine tower. This structure can feature either vertical or inclined pile sleeves, with the latter being utilized when installation occurs via a jack-up drilling rig. Furthermore, both the base width and pile penetration depth can be modified to accommodate specific environmental and soil conditions. The use of these is rare, as they have not proven to be cost-effective options for offshore wind [36]. Figure 22 describes the structure of Tripod foundation.

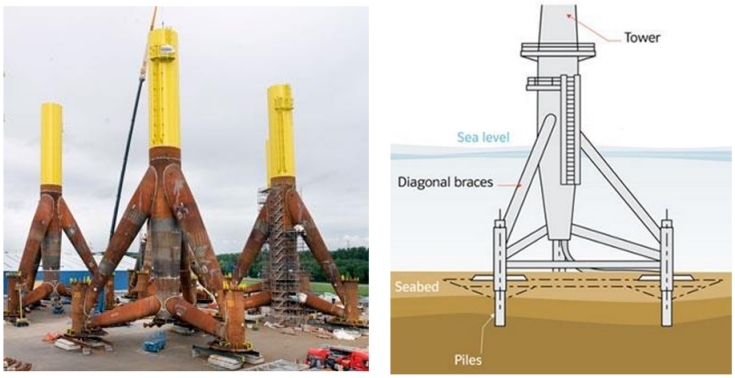

Figure 22: Tripod foundation [37, 38].

2.5.2 Floating foundations

In 2012, offshore wind farms were typically situated at an average water depth of 22 meters, with a mean distance

of 29 kilometers from the coastline. By 2014, proposals had emerged for wind farms positioned as far as 200 kilometers offshore and in depths reaching 215 meters [39]. This indicates a clear trend towards deeper waters, which offers benefits such as reduced visual impact, diminished turbulence, and an expanded area for exploration. Various designs have been developed, with several models already in operation; many of these structures draw inspiration from platforms utilized in the oil industry.

- **Spar Buoy Foundation:** The spar design consists of a substantial deep-draft floating cylinder characterized by a reduced waterplane area, as illustrated in figure 23. Therefore, It can be deployed in water depth usually from 100 meters [40]. It is ballasted to ensure that the center of gravity remains below the center of buoyancy. The structure's foundation is secured through catenary or taut spread mooring lines, utilizing drag or suction anchors for stability. While the spar offers excellent stability and features a more straightforward design compared to semi-submersibles, its elevated structure presents greater

difficulties in terms of fabrication, transportation, and installation [40].

Figure 23: Spar buoy foundation [41].

- **Semi-submersible Foundation:** Semi-submersibles are characterized by several columns that enhance hydrostatic stability, along with multiple pontoons that contribute extra buoyancy. Figure 24 depicts the structure of Semi-submersible foundation. Their positioning is maintained through catenary or taut spread mooring lines paired with drag anchors. Although managing the motion of a semi-submersible presents significant design challenges, these structures are effective across various water depths from around 40 meters [40].

Figure 24: Semi-submersible foundation [42].

- **Tension Leg Platform:** A Tension-Leg Platform (TLP) is a type of platform that is anchored vertically. Similar to semi-submersibles, the TLP comprises columns and pontoons, as described in figure 25. Its distinctive characteristic lies in its mooring system, which utilizes vertical tendons to control heave motion while allowing for lateral movement such as surge, sway, and yaw. The TLP offers strong stability and is suitable for various water depths from around 40 meters; however, its construction and anchoring expenses are greater compared to other floating designs [40].

Furthermore, The Technology Readiness Level (TRL) of floating tension leg platforms (TLPs) currently lags behind that of the other two concepts. Due to their structural stiffness, TLPs are particularly vulnerable to high-frequency dynamic loads, which can induce resonant pitch and heave motions, ultimately resulting in fatigue damage to the tendons. Furthermore, TLPs possess the most costly anchoring system among the three designs, both in terms of fabrication and installation expenses.

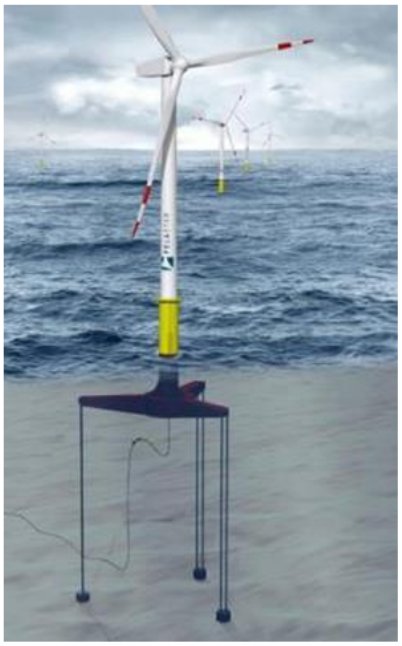

Figure 25: Tension Leg Platform [42].

2.6 Salome software

The model is designed with open source Salome 9.9.0 CAD software. This software is primarily used to design platform's geometry, evaluate the mass, moment of inertia, and the center of mass, evaluate the hydrostatic properties of platform, and design internal structure for ANSYS Mechanical. The most useful feature is that Salome is developed in Python and it is possible to generate a Python code that describes the steps made with the graphical interface. Once the definition of geometry is defined within the Salome GUI, it is possible to export a Python code that reproduces the steps made with the GUI using the option 'Dump study'. With the Python code it is possible to:

- Parametrise the geometry.
- Implement equations such as hydrostatic equilibrium for ballast mass as Python code.
- Call Salome in batch mode externally for automation and optimization purposes.

The design consists of shell elements, which are subsequently imported into Ansys.

2.7 Tension-Leg platform

The platform under study consists of four legs that are anchored in the seabed. The hull provides enough buoyancy to support the weight of the turbine while also creating an upward force that maintains tension on the mooring lines. During an operation, the platform is designed to have a draft of 25 meters below sea water level and 25 meters elevation above sea water level. Since the legs are long, it would be a good practice to support the legs with braces into the main column. The main column is the central column of the structure on top of which the turbine will be connected. The main column also serve as water ballast tank whereas the arms serve as pontoons that can accommodate fixed amount of ballast. The fairleads are placed at the end of the arms on which the mooring lines will be connected. The mooring lines as aforementioned are anchored in seabed of 120 meters depth. Figures 26 and 27 demonstrate the general dimensions and identification of the structure.

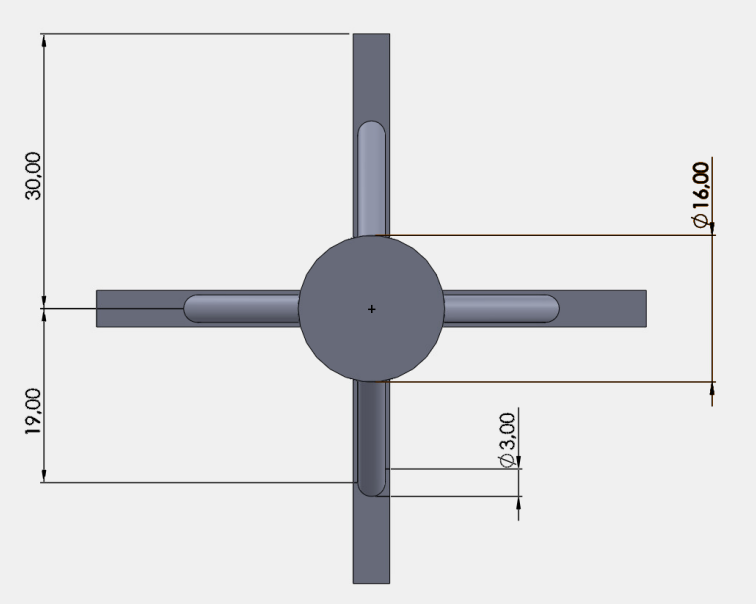

Figure 26: Top view of TLP.

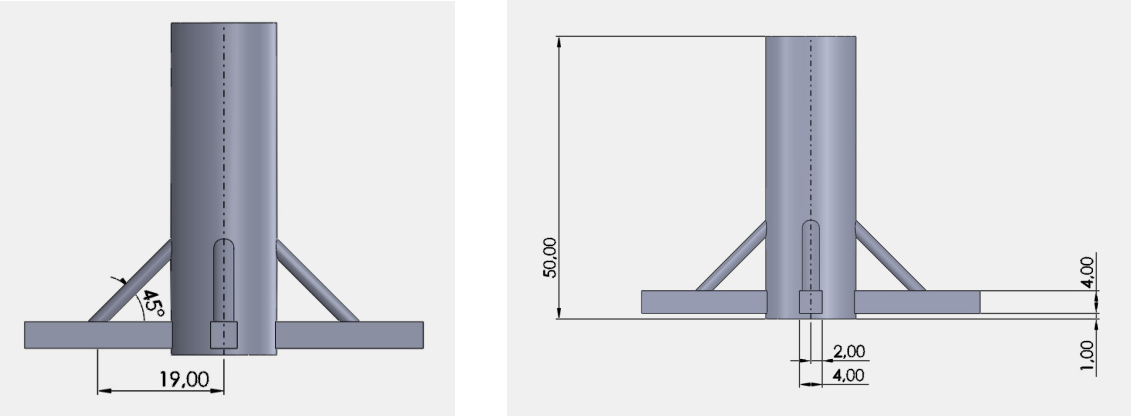

Figure 27: Side view of TLP.

2.7.1 Platform properties

The Tension-Leg platform has a total mass of 4420.46 tons, including steel mass and added water as ballast. The steel mass itself accounts for 2143.57 tons initially. Tension

leg platforms are known for featuring high buoyancy force that maintain legs in tension. The water ballast inside main column tank is at minimum or absent when the buoyancy force is at maximum and the ballast is at maximum when the buoyancy force is at minimum. Thus, the half of water ballast that can be contained without losing buoyancy is initially evaluated to be 2276.9 tons. To compute the buoyancy force, the volume of submerged platform is extracted from Salome software. Furthermore, the main parameters of platform such as ballast mass, inertia and mass of the platform are also extracted from Salome software and are depicted in table 1.

The volume of submerged platform	8.892 m^3
Turbine mass	2416.8 tons
Water ballast mass	2276.9 tons
Platform roll inertia	1.45*10^9 kg m^2
Platform pitch inertia	1.45*10^9 kg m^2
Platform yaw inertia	1.28*10^9 kg m^2

Table 1: Platform main parameters.

In the optimisation process that will be discussed in the following chapters, the buoyancy force is held constant while the optimization algorithm aims at minimizing the

steel mass. In other words, the amount of water ballast inside main column tank will be increased or decreased according to the change in the platform mass, in particular, steel mass. These weights were calculated considering a steel density of 7850 kg/m3 and a water density of 1025 kg/m3.

2.7.2 Structural improvements to the original structure

Study [61] addresses the importance of choice and location of internal stiffeners in reducing global mass and limiting the mechanical stress on Semi-submersible platforms. According to the study, modifications to the design introduce additional support structures at various points of the structure. This includes the stiffeners and girders on the pontoons and the braces, and the radial rings within the main column. The pontoons are reinforced with longitudinal stiffeners and girders while main column is additionally supported with radial stiffeners and radial rings as it can be seen in figures 28 and 29.

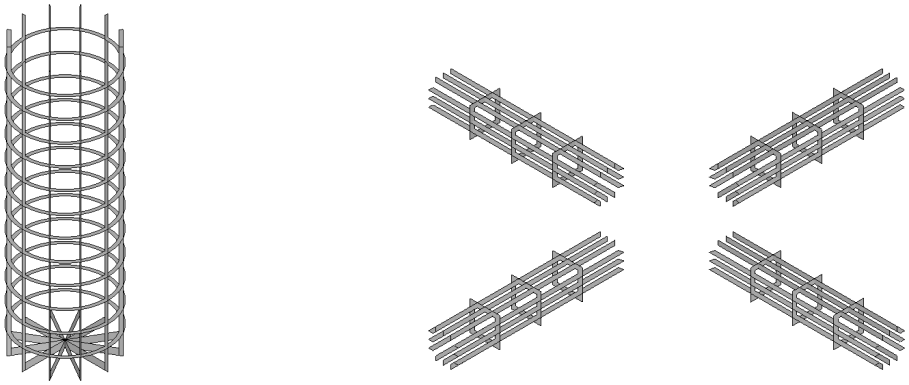

(a) Main column stiffeners. **(b)** Pontoon stiffeners.

Figure 28: Platform reinforcements.

Longitudinal stiffeners are spaced at every 1 meter transversally while radial rings are spaced at 3.6 meters vertically.

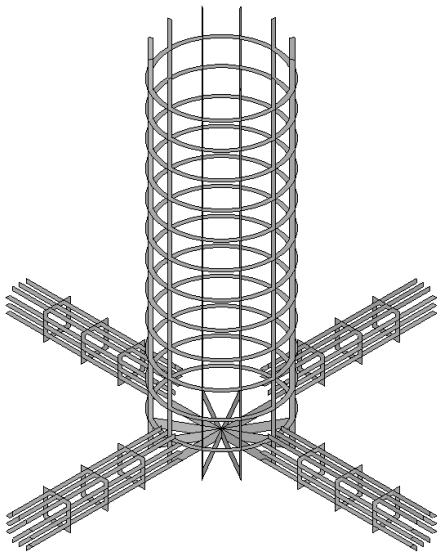

Figure 29: Total stiffeners.

Three girders are placed at each pontoon longitudinally. General dimensions of the internal reinforcing structures are reported in table 2.

Diameter of the rings	3.6 m
Depth of longitudinal stiffeners	0.6 m
Depth of radial stiffeners	1.2 m

Table 2: Stiffeners main parameters.

2.8 Mooring system for Tension Leg Platforms

The mooring layout and configuration of a Tension Leg Platform (TLP) for Floating Offshore Wind Turbines (FOWT) is a critical aspect of the design process, ensuring stability and structural integrity in various environmental conditions [43]. The mooring system of a TLP typically consists of:

1. **Tension Legs:** These are vertical tethers that connect the platform to the seabed. Tension legs are made of high-strength steel or composite materials, providing the necessary stiffness to maintain the platform's stability[43].

2. **Fairleads:** Fairleads are guiding structures that direct the tension legs from the platform to the seabed. They prevent chafing and ensure that the tension legs are aligned properly [43].

3. **Anchor Points:** These are the connection points be-

tween the tension legs and the seabed. They can be anchored using various methods such as suction piles, driven piles, or gravity anchors, depending on the seabed conditions[43].

The mooring layout of a TLP for FOWT is designed to provide stability and minimize platform motions under different environmental loads such as wind, waves, and currents [44]. The layout typically includes:

1. **Symmetrical Arrangement:** Tension legs are usually arranged symmetrically around the platform to distribute the loads evenly and maintain stability.
2. **Spacing and Configuration:** The spacing between tension legs and their configuration depend on various factors such as water depth, environmental conditions, and turbine size. Typically, TLPs for FOWT have four to six tension legs arranged in a square or hexagonal pattern.
3. **Dynamic Positioning System (DPS):** In addition to the mooring system, TLPs may also incorporate a DPS to further enhance stability and control platform motions. The DPS uses thrusters to maintain the

platform's position relative to the wind, waves, and currents.

The mooring layout and configuration of a TLP for FOWT are designed to withstand extreme environmental conditions. Factors such as water depth, wave height, wind speed, and seabed conditions are carefully considered during the design process to ensure the platform's safety and structural integrity.

The mooring layout and configuration of a Tension Leg Platform for Floating Offshore Wind Turbines play a crucial role in ensuring the stability and performance of the platform. By carefully designing the mooring system to withstand various environmental loads, engineers can ensure the safe and efficient operation of offshore wind turbines in deepwater locations

2.9 Finite Element Analysis

Finite element analysis (FEA) is a computerized method for predicting how a product reacts to real-world forces, vibration, heat, fluid flow, and other physical effects [45].

Finite element analysis shows whether a product will break, wear out, or work the way it was designed [73]. In the product development process, FEA simulation is used to predict what is going to happen when the product is used in its real world application to ensure it achieves whatever tasks that component needs to perform safely and efficiently [73].

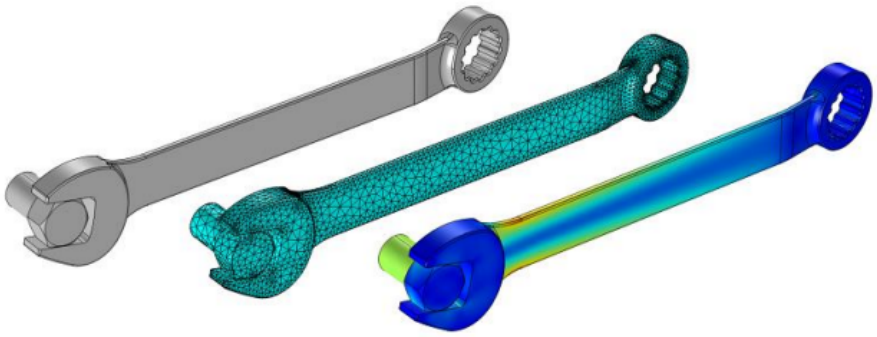

Figure 30: Finite Element analysis procedure [46].

ANSYS is one of the popular engineering simulation software used for modeling, analysis and simulation of complex problems in various industries [47]. Its capabilities to analyse structural mechanics, heat transfer, and fluid flow are exercised by applying methods such as finite element analysis (FEA), computational fluid dynamics (CFD) and electromagnetics. ANSYS is prominent for conducting multi-physics simulations, which allows to analyze cou-

pled physics problems such as fluid-structure interaction or thermal-mechanical features. With an intuitive interface and robust solvers, this software is used to go from design, optimization and to real-world performance. ANSYS reduces prototyping costs and speeds up innovation by delivering the best insight into all engineering systems.

Chapter 3

METHODS

3.1 Tower and Turbine properties

This research considered the NREL IA15 MW Reference Turbine [48]. Table 3 describes main parameters of the reference turbine.

Cut-in wind speed	3 m/s
Rated wind speed	11.4 m/s
Cut-out wind speed	25 m/s
Rotor diameter	240 m
Hub height	150 m
Tower height	129.386 m
Tower mass	1466.7 tons
Blade length	117 m
Blade mass	6850.8 tons
Rotor nacelle assembly mass	1017 tons
Electrical generator efficiency	0.9658
Cut-in rotor speed	5 rpm
Cut-out rotor speed	7.56 rpm

Table 3: Turbine properties [48].

It is an upwind 3-bladed turbine, also used as a reference for research study [61].

3.2 Material properties

The platform material is steel, namely S355 steel. This material has a Young modulus of 210 Pa and a shear modulus of 80.8 GPa. Steel's density is 7 850 kg/m^3.The S355 steel yield strength is considered to be 355 MPa [50]. For the analyses, the density of water was also needed, thus it was defined as 1025 kg/m^3 [51].

3.3 OpenFAST software

Offshore structures are subjected to hydrostatic, hydrodynamic and aerodynamic loadings, usually due to the wind, waves and tides. In order to produce the correct inputs to use as loads on the Finite Element Analysis, the OpenFAST software from NREL was used [52].
OpenFAST is a multi-physics, multi-fidelity tool for sim-

ulating the coupled dynamic response of wind turbines [52].

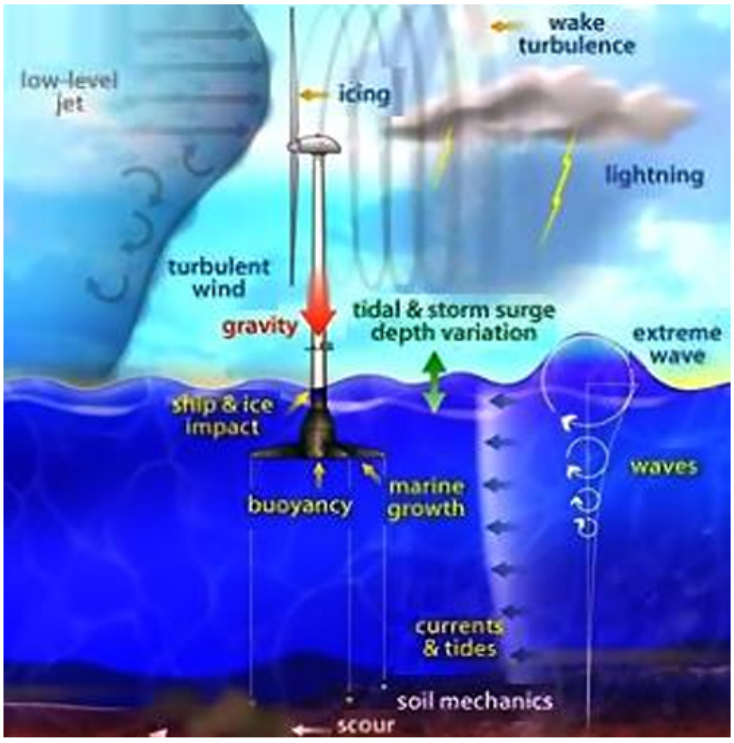

Figure 31: OpenFAST envirionment conditions [62].

OpenFAST is the framework (that couples computational modules for aerodynamics, hydrodynamics for offshore structures, control and electrical system (servo) dynamics, and structural dynamics to enable coupled nonlinear aero-hydro-servo-elastic simulation in the time domain [52]. OpenFAST enables the analysis of a range of wind turbine configurations, including two- or three-blade horizontal-

axis rotor, pitch or stall regulation, rigid or teetering hub, upwind or downwind rotor, and lattice or tubular tower. The wind turbine can be modeled on land or offshore on fixed-bottom or floating substructures [52].

FAST consists of multiple modules, each dedicated to simulating specific effects that interact with the structure. The modules utilized in this research include:

- **ElastoDyn:** simulates the physical properties of the structure and the initial operating conditions of the turbine [53].
- **ServoDyn:** manages the configuration of the turbine's control systems [53];
- **Inflow:** Analyzes wind inflow data, facilitating the simulation of aero-elastic effects on horizontal-axis wind turbinesg [54];
- **AeroDyn:** A time-domain module for wind turbine aerodynamics that allows for the simulation of aero-elastic interactions affecting horizontal-axis wind turbines [55];
- **HydroDyn:** calculates hydrodynamic loads [56].

- **MoorDyn:** A lumped-mass model for mooring lines that predicts the dynamics of standard mooring systems [57].

3.4 Coordinate systems for the analysis

The motions assessed are relative to a coordinates system that is pre-defined. The most common type of coordinate systems is described in figure 32.

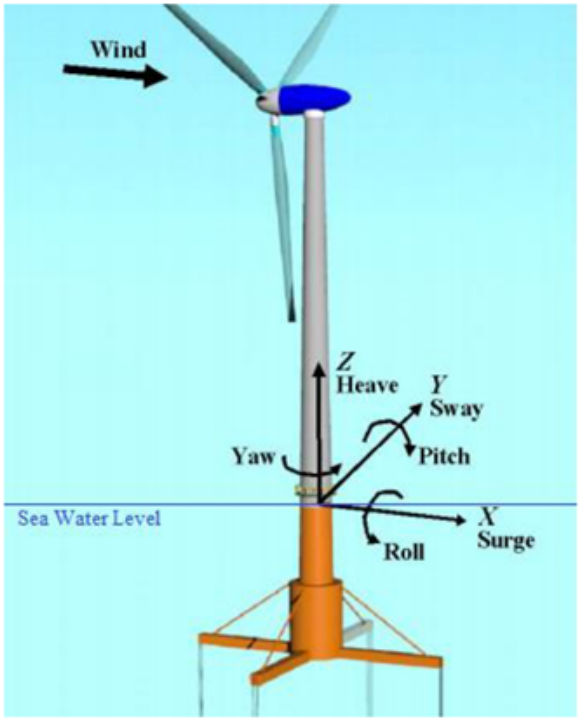

Figure 32: Coordinate system for analysis [56].

The rotation movement around each axis are also shown and are named as Yaw, Pitch and Roll. Yaw is the rotation around the Z axis, Pitch is around Y and Roll is around X [56].

3.5 Simulation parameters

One of the critical components of the simulation is the behavior of the sea, as it generates the most significant destructive forces impacting the structure. The modeling of hydrodynamic effects incorporates both incident-wave kinematics and various hydrodynamic loading models. These loads arise from integrating the dynamic water pressure across the wetted surfaces of the floating platform, encompassing inertia, linear drag, buoyancy, incident-wave scattering, sea currents, and nonlinear phenomena [56].

In simulations such as those conducted by OpenFAST's HydroDyn module, two primary methodologies utilized for modeling water waves are regular and irregular waves.

- Regular waves: also known as deterministic or peri-

odic waves, represent an idealized wave form with consistent characteristics. These waves are described by a simple sinusoidal equation [60]:

$$V(x,t) = Acos(kx - \omega t + \phi) \tag{1}$$

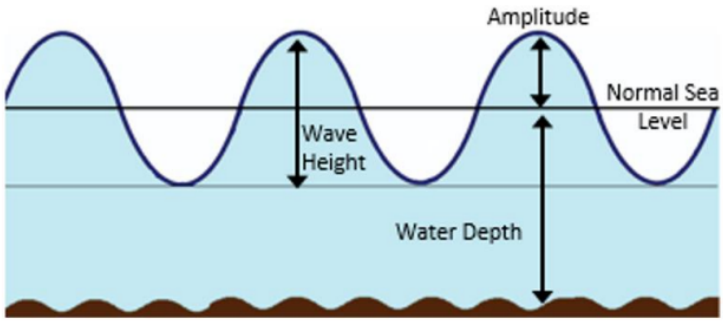

Figure 33: Mathematical wave simplification [72].

- Irregular waves: also known as stochastic or random waves, offer a more realistic representation of ocean conditions. These waves are modeled using wave spectra that describe the distribution of wave energy across various frequencies [60].

Wave spectra provide a statistical description of sea states. Commonly used spectra include:

- Pierson-Moskowitz (PM): Represents fully developed seas in deep water with a steady wind.
- JONSWAP (Joint North Sea Wave Project): Extends

the PM spectrum by adding a peak enhancement factor, making it suitable for wind-driven waves in fetch-limited conditions.

- Bretschneider Spectrum: Often used for swell-dominated seas.

The wave elevation for irregular waves is obtained by summing a series of sinusoidal waves with different frequencies and amplitudes:

$$V(x,t) = \sum_{i=1}^{N} A_i cos(k_i x - \omega_i t + \phi_i) \tag{2}$$

Irregular wave modeling captures the randomness of ocean waves, reflecting the variability in wave height, period, and direction observed in real seas and enables simulation of complex interactions between waves and offshore structures. It is essential for fatigue analysis, survivability studies, and system optimization under real-world conditions. Hence, it is used in long-term performance predictions and extreme condition simulations. In general, regular wave modeling serves as a baseline to understand fundamental system dynamics and verify

simulation tools while irregular wave modeling provide the variability needed to predict long-term performance and structural integrity under realistic sea states, which is crucial for offshore wind turbines and floating platforms. By integrating both wave types, the module " HydroDyn " ensures flexibility in analyzing offshore structures across a wide range of environmental conditions.

In order to use accurate data of weather and sea conditions, a real specific location had to be chosen. For this research, a site located off the western coast of Italy in the Mediterranean Sea, near the island of Sardinia is selected.

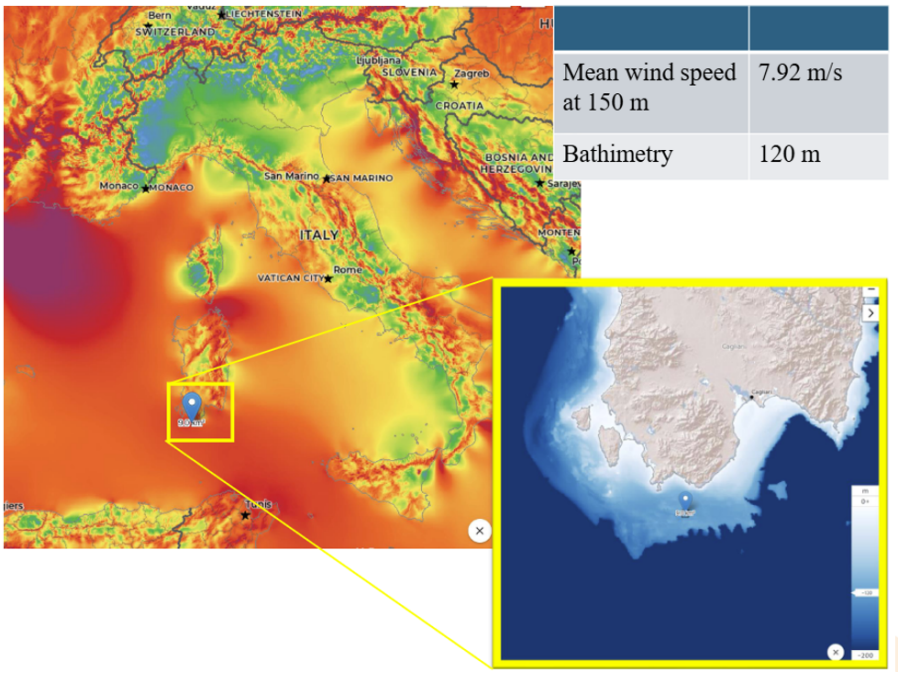

Mean wind speed at 150 m	7.92 m/s
Bathimetry	120 m

Figure 34: Selected site location [75].

The specific coordinates appear to target a location around 96 kilometers offshore, as indicated by the pin marker in map 34. Several quantities may be used to describe the random behavior of waves stochastically, being the most important the Significant Wave Height and the Peak Wave Period. The Significant Wave Height, H_s, is the mean of the highest third of the waves in a time-series that represents a certain sea state. The Peak Wave Period, T_p, is the wave period with the highest energy [59]. For the selected site, the parameters are derived accordingly in equation 3.

$$\begin{aligned} H_s &= 1.57m \\ T_p &= 6.97s \end{aligned} \tag{3}$$

Various theories have been developed to calculate hydrodynamic loads on floating structures, including TLP. For example, The potential-flow theory is applicable to substructures or their components that are relatively large compared to a typical wavelength [62]. This theory encompasses aspects such as linear hydrostatic restoration, along with the contributions of added mass and damping

resulting from linear wave radiation and incident-wave excitation [62].

Conversely, strip theory is more suited for substructures or their members that have smaller diameters in relation to a standard wavelength [62]. The hydrodynamic loads derived from this approach can be applied across multiple interconnected elements—whether they are inclined or tapered—and originate directly from the undisturbed kinematics of waves and currents at the structure's original position [62]. These loads incorporate a relative version of Morison's Equation addressing distributed fluid-inertia, added-mass, and viscous-drag factors. Moreover, strip theory accommodates ballasting members and accounts for marine growth effects [62]. It is also possible to integrate potential-flow theory with strip-theory methods when necessary [62]. This hybrid approach becomes particularly beneficial if there is an need to amplify hydrodynamic loads predicted by potential-flow due to flow separation effects; this can be achieved by incorporating the viscous-drag component from strip-theory into the solution provided by potential-flow analysis [62].

3.6 Structural analysis

The structure is subjected to several static loads such as:

1. Hydrostatic pressure from sea water.
2. Forces and moments resulting from static aerodynamic thrust and the weight of the turbine.
3. Loads from the mooring lines.
4. Hydrostatic pressure from internal ballast.

The loads transferred between the tower and mooring lines are computed in OpenFAST time-domain simulations.

As discussed in the previous chapters, a particular amount of water ballast is required to maintain required draft from design. The structural steel mass is obtained by setting the thicknesses for each group of shell elements. The calculation of ballast is demonstrated in equation 4, where $V_{Submerged}$ is the volume of submerged platform, M_{Steel} is the structural steel mass, $M_{Waterballast}$ is the fixed ballast inside the pontoons and $M_{Turbine}$ is the mass of the turbine.

$$M_{Ballast} = \rho * V_{Submerged} - M_{Steel} - M_{Waterballast} - M_{Turbine} \quad (4)$$

The centre of mass of the platform is then evaluated by summing the centre of mass (CoM) of steel, the centre of mass of water ballast in the pontoons, additional ballast inside the main column and dividing the result by total mass. It is assumed that the ballast density is 1025 $kg * m^{-3}$ (generic water). The ballast is represented as an internal hydrostatic pressure. This internal pressure is advantageous for the structural integrity of the platform because it counteracts the external hydrostatic pressure exerted by seawater [61]. The level of this internal pressure corresponds to the height of the ballast. Additionally, the model includes the gravitational force resulting from the mass of the steel. To factor in the aerodynamic thrust forces and moments, as well as the self-weight of the wind turbine, the platform's orientation is adjusted relative to the sea water level (SWL) [61]. These specific values are derived from time-domain simulations conducted in OpenFAST. The distribution of hydrostatic pressure, influenced by the pitch, roll angles, and heave, primar-

ily governs the tower's reaction forces. These forces are essential as they bear the weight of the turbine and counteract the pitching and rolling moments generated by the turbine's thrust. The pontoons in the design do not experience hydrostatic pressure due to the presence of water ballast within them. It is assumed that there is a balance between the internal and external pressures [61].

3.6.1 Hydrostatic stiffness of mooring lines.

The stiffness of the mooring is obtained by (Al-Solihat and Nahon, Stiffness of slack and taut moorings, 2016):

$$K_{11}^{moor} = \frac{B}{FL_D} \tag{5}$$

$$K_{33}^{moor} = n\frac{EA}{L} \tag{6}$$

$$K_{15}^{moor} = (\frac{n}{2})\frac{EA}{L}FL_x^2 + B\frac{FL_z^2}{FL_D} + BFL_z \tag{7}$$

$$K_{66}^{moor} = B\frac{FL_z}{FL_D} \tag{8}$$

$$K_{55}^{moor} = B\frac{FL_z^2}{FL_D} \tag{9}$$

The variables in the equations from 5 to 9 are demonstrated in figure 35, where force T represents thrust force

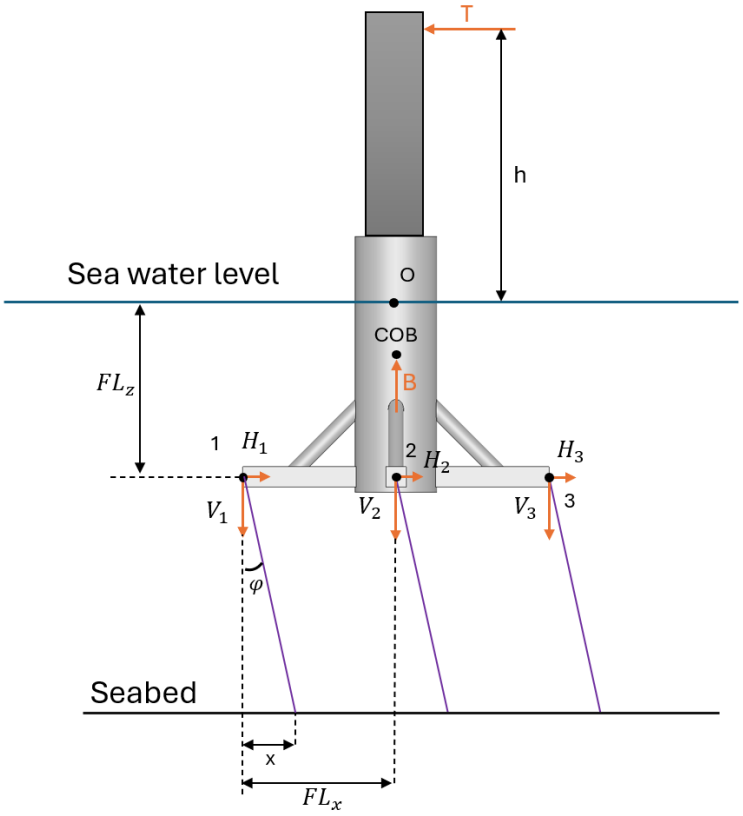

Figure 35: Structural analysis of the platform.

generated by turbine, the force B represents Buoyancy force, and the forces V_i and H_i represent the reaction forces on the fairleads.

3.6.2 Preliminary mooring line design

The design of Tension Leg Platform is not self-stabilizable without mooring system. Hence, initial considerations about mooring system must be taken into account to derive static and dynamic response of the platform. The mooring lines of Tension Leg Platform are kept in tension. So, there are constraints on the frequency responses of the system in pitch, roll and heave degrees of freedom, which should be below the natural period of the waves. To be more precise, the natural periods in both heave and pitch motions should be below 3 seconds. A natural period of 3 seconds is selected specifically since the wave natural period in Mediterranean sea is estimated to be from 4 to 13 seconds. The dimensioning of mooring line is based on the evaluation of line elasticity to achieve the required natural periods in pitch and heave degrees of freedom, which are calculated as following:

$$T_3 = 2\pi\sqrt{\frac{M + A_{33}}{K_{33}^{hydro} + K_{33}^{moor}}} < T_3^{max} = 3 \tag{10}$$

$$K_{33}^{max} = \frac{M + A_{33}}{(\frac{T_3^{max}}{2\pi})^2} - K_{33}^{hydro} = n\frac{EA}{L} \tag{11}$$

$$EA_3 = K_{33}^{max}\frac{L}{n} \tag{12}$$

$$T_5 = 2\pi\sqrt{\frac{I + A_{55}}{K_{55}^{hydro} + K_{55}^{moor}}} < T_5^{max} = 3 \tag{13}$$

$$K_{55}^{max} = \frac{I + A_{55}}{(\frac{T_5^{max}}{2\pi})^2} - K_{55}^{hydro} \tag{14}$$

$$K_{55}^{max} = \frac{I + A_{55}}{(\frac{T_5^{max}}{2\pi})^2} - K_{55}^{hydro} =$$
$$= \frac{n}{2}\frac{EA}{L}FL_x^2 + B\frac{FL_z^2}{FL_D} + BFL_z \tag{15}$$

$$EA_5 = (K_{55}^{max} - B\frac{FL_z^2}{FL_D} - BFL_z)\frac{2L}{nFL_x^2} \tag{16}$$

$$EA = max(EA_3, EA_5) \tag{17}$$

As can be noted, the added mass is needed to evaluate the mooring stiffness. The added mass at infinite frequency is used in this context, and the final RAO and static pitch angle is based on EA evaluated before.

3.7 Buckling analysis

Buckling analysis is a vital method for assessing the stability of structures subjected to axial loads. It provides an estimate of the load level at which a structure, be it a column, beam or shell will enter an unstable state while deforming rapidly and might collapse. This assessment provides critical buckling loads and related buckling modes, allowing for engineering confirmation that applied forces do not result in collapse. Eigenvalue analysis for idealized linear systems, or nonlinear analysis considering material imperfections and large geometries are common methods used to perform buckling analysis. This is critical in fields as varied from aerospace to civil engineering where stability of the structure is of paramount importance.

3.8 Structural optimization

Structural optimization by Finite Element Method(FEM) is a computational method for structural refinement

where geometry, material or other attributes are optimized within given constraints like strength, stiffness or weight. Combining FEM with optimization algorithms allows engineers to evaluate the impact of design alterations on structural performance under applied loads, enabling iterative refinement of a design based on specified goals such as reducing material usage, diminishing stress concentrations or improving stability. In this process, first a objective function is defined, then FE analysis will be conducted to analyze the responses for the structure based on its geometry, sensitivity analysis which tells us which design variable has maximum contribution in the response of interest and algorithm(e.g. gradient based or evolutionary)in optimizing the structure. These applications cover lightweight aerospace part until heavy duty offshore platform. With respect to floating offshore wind turbines, such structural optimization can optimize the design of a tension leg platform to find the lightest possible solution while still maintaining stability and robustness against environmental loads.

3.8.1 Objectives and algorithm

Optimisation definition The optimisation process utilized in this study employs the "scipy.optimize.fmin" function from the SciPy library ("Fmin Function" 2024). This function implements the Nelder-Mead algorithm, which is a gradient-based optimizer designed to locate the local minimum of a given function. The function is utilized in the optimization process to adjust the thicknesses of various structural components, including the main column, braces, and internal stiffeners. To streamline the process, the positions of the internal stiffeners are kept fixed during optimization. This decision serves two main purposes: first, it reduces the number of input variables, which in this study ranges from 4 to 10; second, it ensures a consistent geometry and mesh throughout all iterations, thereby simplifying the workflow.

The optimization process aims to minimize the total mass of structural steel while incorporating constraints related to yield stress and buckling strength. Yield stress constraints are evaluated by comparing the Von Mises stress to the steel's yield stress, typically 355 MPa, a standard value for offshore wind platforms [72], [74]. A

safety factor of 1.5 is applied, resulting in a stress limit of 235 MPa.

Buckling constraints are examined via eigenvalue buckling analysis, which entails resolving an eigenvalue problem that arises from the equilibrium equations of the structure. Here, the eigenvalue—often referred to as the load multiplier—indicates how much a given load must be adjusted in order to induce a loss of stiffness and stability within the structure. This type of analysis is especially vital for floating wind platforms, where shell elements predominantly experience compressive stresses, rendering them susceptible to buckling instabilities. To ensure safety during this evaluation, a factor of 1.5 is incorporated into the load multiplier associated with the initial buckling mode.

The objective function incorporates these constraints as penalties, alongside the assessment of steel mass. These penalties are formulated as parabolic functions based on the specific constraint. The objective function is defined in equations 18, 19, 20, 21 and 22 where σ represents the Von Mises stress and LM is the load multiplier of the first buckling mode [61].

$$OBJ = M_{STEEL} + OBJ_{YIELD} + OBJ_{BUCK} \tag{18}$$

$$OBJ_{YIELD} = 0.4\sigma^2 + 112\sigma + 9000 \qquad if \quad \sigma > 235 \tag{19}$$

$$OBJ_{YIELD} = 0 \qquad if \quad \sigma < 235 \tag{20}$$

$$OBJ_{BUCK} = 16032LM^2 - 48080LM + 36048 \qquad if \quad LM < 1.5 \tag{21}$$

$$OBJ_{BUCK} = 0 \qquad if \quad LM > 1.5 \tag{22}$$

3.9 Boundary conditions

Boundary conditions in simulations define the limitations and interactions applied to a model to replicate real-world scenarios. They specify how forces, displacements, temperatures, or other physical factors are constrained or applied to the system. These can include displacement constraints (such as fixed supports or rollers), applied forces or pressures (e.g., point loads or distributed loads), thermal conditions (like fixed temperatures or heat transfer), and contact conditions (such as friction or separation between surfaces). Properly defining boundary conditions is crucial for ensuring the accuracy and realism

of the simulation, as they directly affect how the model behaves under different loads and environmental factors, ensuring that the results are physically meaningful and computationally stable.

To prevent rigid body motion, two constraint methods were considered: inertial relief and a fixed constraint at the interface between the tower and the platform. Inertial relief applies acceleration forces on the mass elements to balance unbalanced forces so that small resultant force which could cause movement does not occur. Imperfections in force application would, of course, cause some unwanted acceleration, and the key is that this must be as little as possible [61]. Simply, due to these aspects inertial relief is usually the way to go for modeling floater constraints without over-constraining the model. However, the pre-stress distribution that can be generated by inertial relief in ANSYS Mechanical cannot be used as part of an eigenvalue buckling analysis [61]. Thus a constrained was imposed around the perimeter of the base of the tower-platform interface. Though such an approach can keep the stability of the structure, it can also cause deviation in stress distribution since the tower

base acting as rigid and result into fictitious stress concentrations within this area [61]. This approach should be cautionary to not introduce unrealistic results. The fairleads have a square surface attached corresponding to the cross-sectional area of each arm moored on either side of the platform, and mooring loads are applied as forces distributed across this mooring bent as shown in figure 37 while figure 36 describes the implementation of hydrostatic pressure and gravity acceleration in ANSYS.

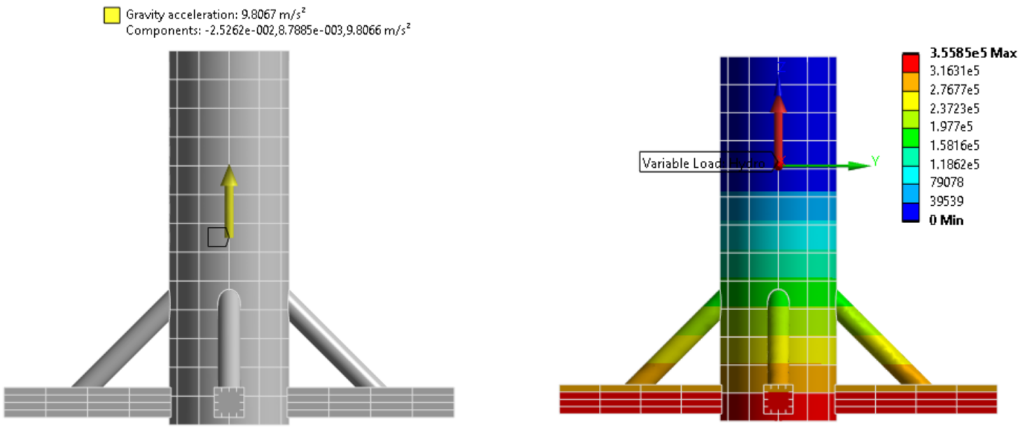

Figure 36: Implementation of gravity acceleration (left) and hydrostatic pressure (right)

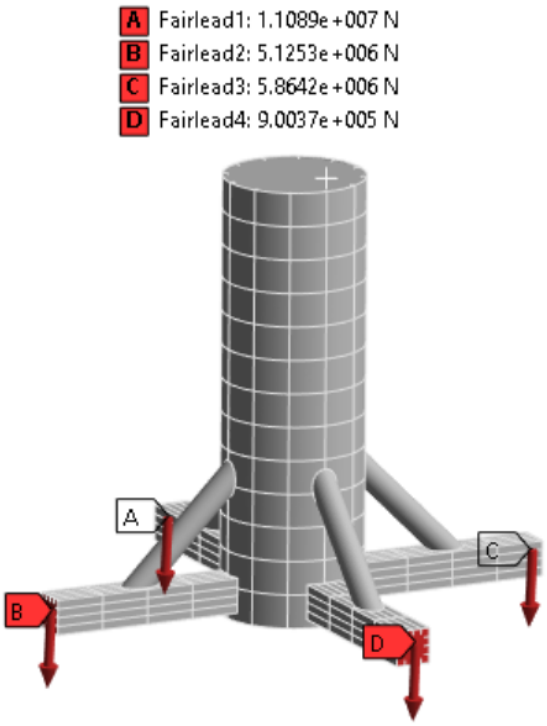

Figure 37: Forces applied on the fairleads.

Additional constraints are set to the amount of ballast present inside the main column in order to avoid slackening of the mooring lines. For this purpose, slackening force is to be defined in eq 25. The maximum amount of ballast, given as a percentage, that satisfies the aforementioned constraint is given in equation 29.

$$\phi = atan(\frac{x}{FL_D}) \tag{23}$$

The overturning moment is described as:

$$M_o = T(h + FL_z) - K_{55}^{hydro}\alpha \tag{24}$$

$$F_{slack} = \frac{B}{n} - \frac{M_o}{(FL_x\frac{n}{2})}cos\phi + \frac{T}{n}sin\phi > 0 \tag{25}$$

Assuming that $\alpha = 0$ and $\phi = 0$,

$$F_{slack} = \frac{B}{4} - \frac{M_o}{2FL_x} > 0 \tag{26}$$

In other words, to avoid slackening

$$B > \frac{2M_o}{FL_x} \tag{27}$$

Thus, equation 27 imposes lower bound on the buoyancy force, which in its turn imposes upper bound on the amount of ballast that can be present inside the main column in the equation 29.

$$B = (1 - perc)(\rho * V_{submerged} - M_{Steel} - M_{Turbine}) > \frac{2M_o}{FL_x} \tag{28}$$

The $perc$ variable in the equation 29 represents the relative amount of ballast with respect to the maximum amount

of ballast.

$$perc^{max} = 1 - \frac{2T(h + FL_z)}{(\rho * V_{submerged} - M_{Steel} - M_{Turbine})gFL_x} \tag{29}$$

Chapter 4

RESULTS

4.1 OpenFAST static simulation results

The OpenFAST model assesses the heave, pitch, and roll angles essential for simulating hydrostatic pressure distribution and the mooring forces exerted on the fairleads [61]. Furthermore, it analyzes the forces and moments at the base of the tower to facilitate comparative analysis [61]. The simulation is carried out for 100 seconds with integration time step of 0.1 seconds and additional linear damping, aiming to achieve steady-state values. These simulations take place under still water conditions and a constant wind speed corresponding to the rated wind speed of 10.56 m/s. Integration time step is to be chosen with care since the smaller is the time step, the longer is the computation time.

The results of OpenFAST simulation are reported in figures 38 and 39, where tension forces in the mooring lines

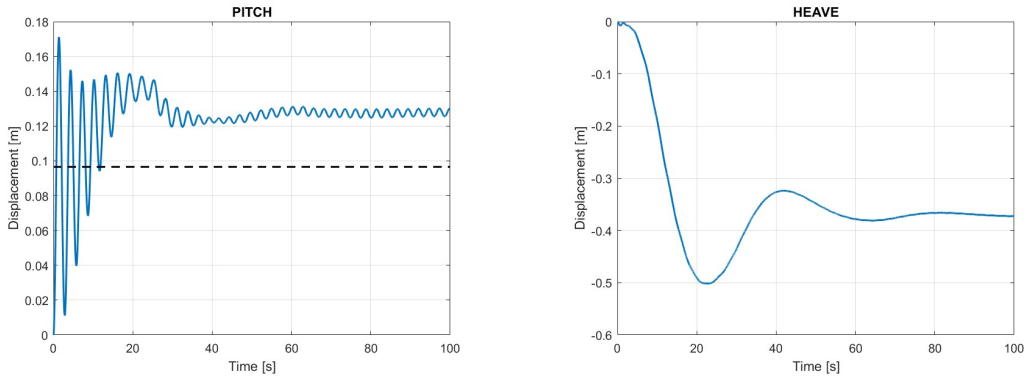

Figure 38: Pitch motion on the left and Heave motion on the right.

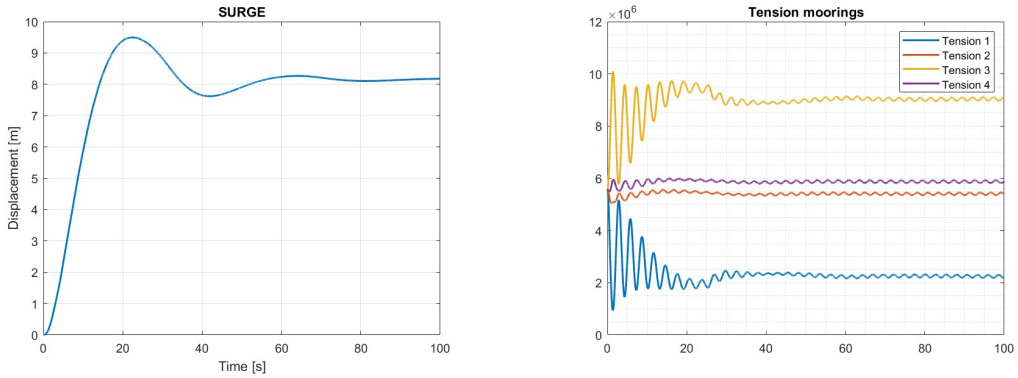

(a) Surge motion.

(b) Tension forces on the mooring lines.

Figure 39: Surge motion on the left and Tension forces on the mooring lines on the right.

and the pitch, heave and surge motions are depicted.

Afterwards, The analysis involves running multiple simulations with varying center of mass (CoM) values for the platform. The results of these simulations are analyzed through linear interpolation, as the relationships between the variables and the platform's CoM are mostly linear, with minor non-linearity introduced by the mooring system.

$$\begin{cases} Heave = -0.000016COM - 0.379823 \\ Roll = 0.000192COM + 0.055555 \\ Pitch = 0.000103CO+, 0.149849 \end{cases} \quad (31)$$

$$\begin{cases} F_{x,1} = 98.67COM - 58537.34 \\ F_{x,2} = 105.28COM - 462960.97 \\ F_{x,3} = -257.91COM - 1006576.64 \\ F_{x,4} = 65.48COM - 503303 \end{cases} \quad (32)$$

$$\begin{cases} F_{y,1} = -8.007897COM - 3138.632587 \\ F_{y,2} = -39.266893COM - 9673.368915 \\ F_{y,3} = 30.834666COM + 10728.752926 \\ F_{y,4} = -47.732907COM - 11062.651988 \end{cases} \quad (33)$$

$$\begin{cases} F_{z,1} = 1025.689724COM - 875841.685561 \\ F_{z,2} = 1680.427829COM - 5067305.709728 \\ F_{z,3} = -2763.894442COM - 11103949.714518 \\ F_{z,4} = 29.688125COM - 5841754.630139 \end{cases} \quad (34)$$

Four CoM values, ranging from -13 to -16 meters below sea

water level, are used for this analysis. The interpolation equations for these key values are provided for reference in equations from 31 to 34. Subsequently, the mooring forces are rotated from the global reference system of the SWL to the platform's local reference system.

4.2 Structural simulation results

The initial simulation is carried out with the thickness of each group of shell elements set to 4 cm. Furthermore, the platform is considered reinforced with internal stiffeners in this simulation. Figures 40 and 41 demonstrate the results of the Von Mises stress and total deformation. This preliminary structural simulation is to highlight the critical areas of stress distributions. In other words, It can be demonstrated from the figures that the stress is highly concentrated on one of the connection joints between braces and main column and the bottom of the structure. This issue can be attributed to consequence of setting low thickness for main column group elements.

.

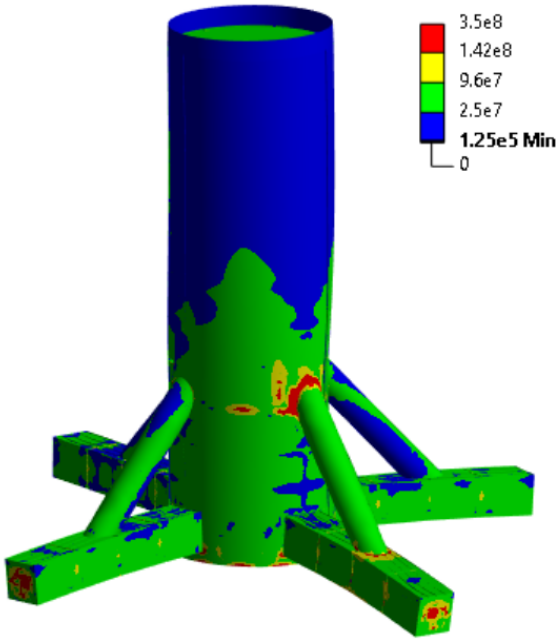

Figure 40: Stress distribution of the platform evaluated in the first structural simulation.

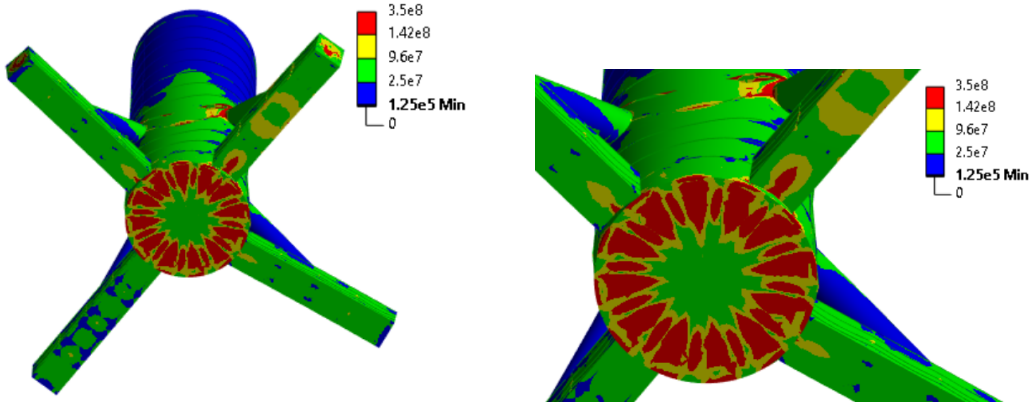

Figure 41: Critical areas of stress distribution.

Furthermore, the overturning moment causes high reaction force on one of the arms, the result of which can be highlighted on figure 42 of total evaluated deformation. It is a good practice to note the total deformation that

structure experienced, amounts for 0.1441 m.

.

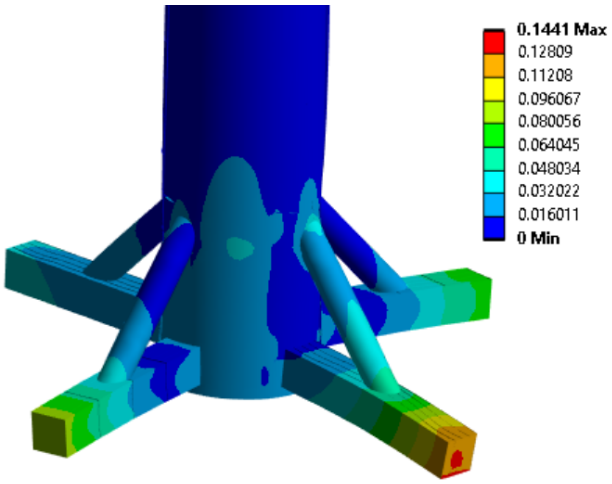

Figure 42: Total deformation calculated in the first structural simulation.

4.3 Structural optimization results

The optimization process begins with focusing on the external geometry of the structure, which consists of shell elements. Internally, the only components considered are the walls that separate the cylinders from the pontoons and braces. The thicknesses of shell elements are categorized in three groups such as main column, pontoons, and braces. The mesh size is selected to be 0.5 meters, which generates around 30875 nodes. The initial thickness of each group is set to 4 centimeters.

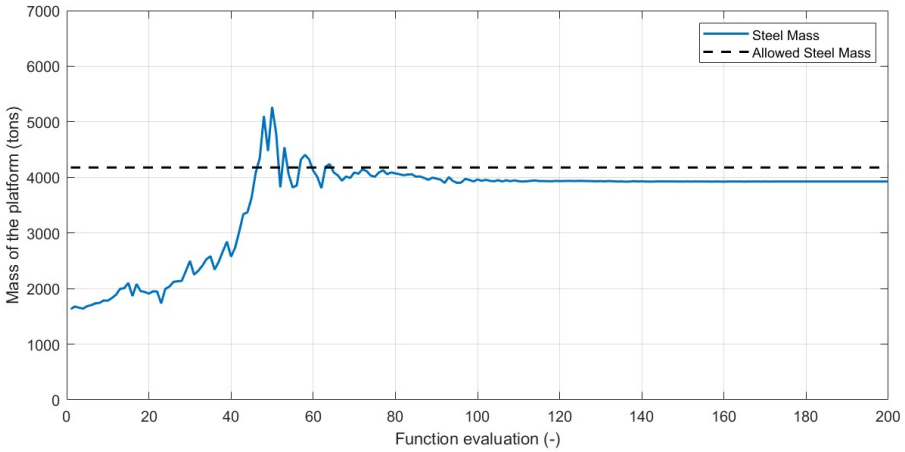

Figure 43: First optimization results of structural steel mass.

One of the most important consideration in the initial optimization is that the platform is not reinforced with internal stiffeners. The results of this optimization allow to demonstrate the critical importance of reinforcements in the structural performance of the platform. Figure 43 presents a graphical representation of how the steel masss evolves during the optimisation process whereas figure 44 depicts the evolution of Von Mises stress and Load multiplier. As it can be seen from figures, the optimisation algorithm reached a point of convergence after approximately 100 iterations. Although the results indicate that the steel mass amounts to be slightly lower than allowed steel mass, the steel mass accounts to be significantly high.

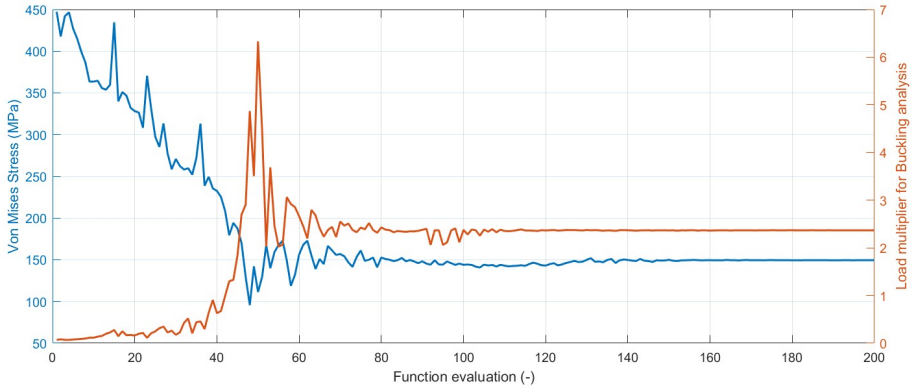

Figure 44: Optimisation results of Von Mises stress and Load Multiplier.

Furthermore, the final values for thickness of each group is demonstrated in the figure 45, where the main column thickness amounts 14 centimeters.

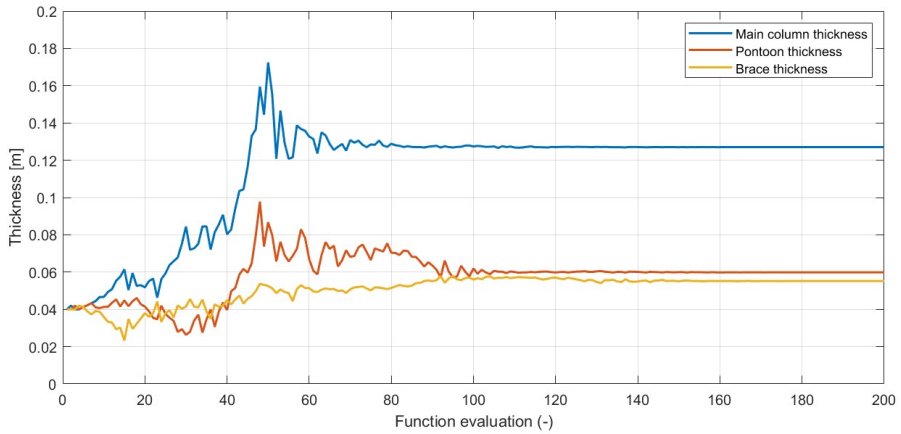

Figure 45: First optimisation results of thicknesses of surface groups.

Figure 46 shows the distribution of stress on the optimised platform. This stress map highlights that the bottoms of the cylindrical columns and arms are critical areas in terms of design and therefore require reinforcements.

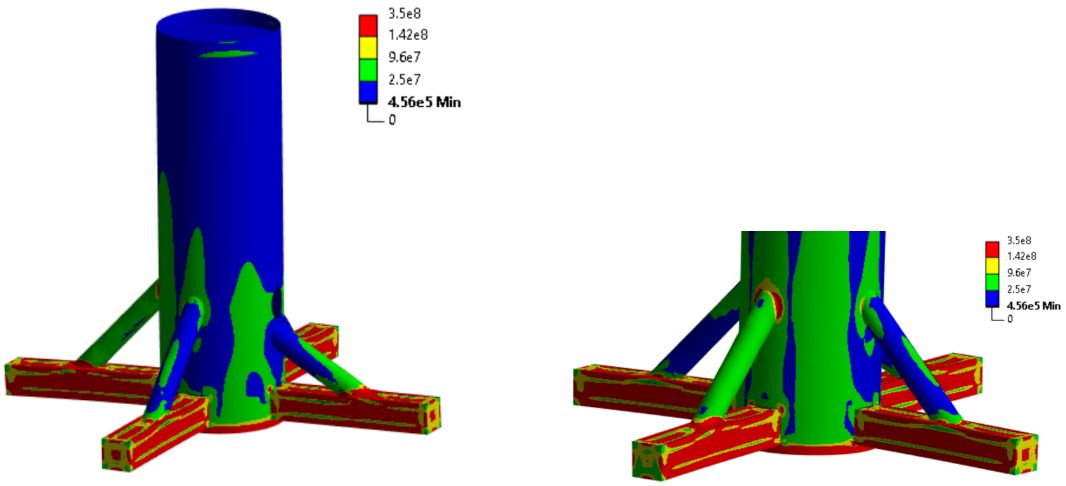

Figure 46: Final stress distribution evaluated at the end of the optimisation.

These areas require a substantial increase in material thickness to withstand deformation — specifically, 14 cm for main columns and 6 cm for the pontoons. In response to these insights, a second iteration of design optimisation is undertaken. This iteration involves adding reinforcements and adjusting the thicknesses of various structural elements to address the identified weaknesses. The platform is then re-optimised based on these new specifications. In the second optimisation attempt, additional stiffeners are introduced to the main and external columns of the structure. These stiffeners are specifically designed to counteract the hydrostatic pressure at the bottom of the columns, as described before. To facilitate the optimization, the thicknesses of reinforcements are

considered in the groups where they have been placed. The progress of this optimisation is charted in Figure 47, The addition of these new stiffeners significantly reduced the thickness required for the columns. This led to a substantial reduction in the overall mass of the platform, bringing it down from 3961 tons to 2870 tons. Moreover, it can be demonstrated from the graphs that the algorithm converged after around 100 iterations.

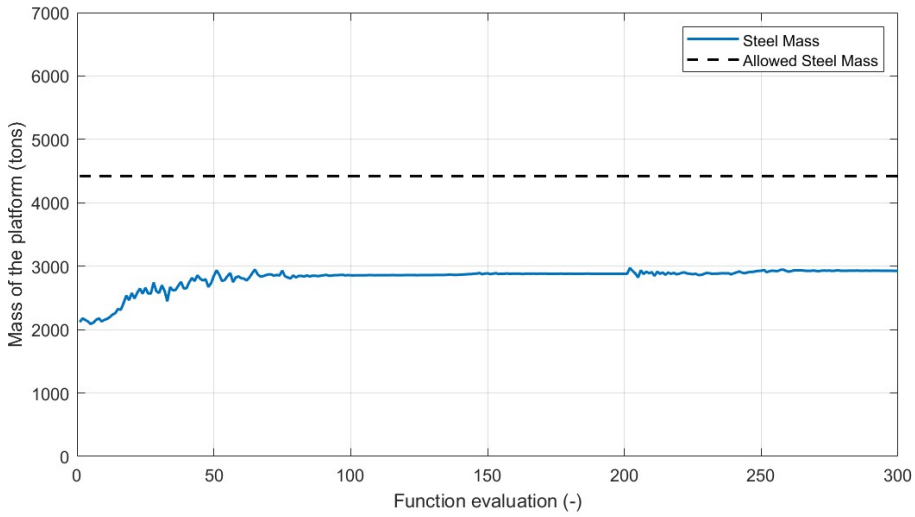

Figure 47: Second optimization results of structural steel mass.

At the 201st iteration, the optimisation algorithm "fmin" was restarted. This restart is evident in Figures 47, 48 and 49 as a perturbation in the data. This step was necessary to move the optimisation process out of a local minimum where it had become stuck. This situation highlights a

common issue with the gradient-based algorithm, namely its difficulty in consistently converging to a global minimum [61]. It can be clearly illustrated in figure 48 where Load multiplier initially converges at about 3.1 and finally reaches to 2.5 after perturbation.

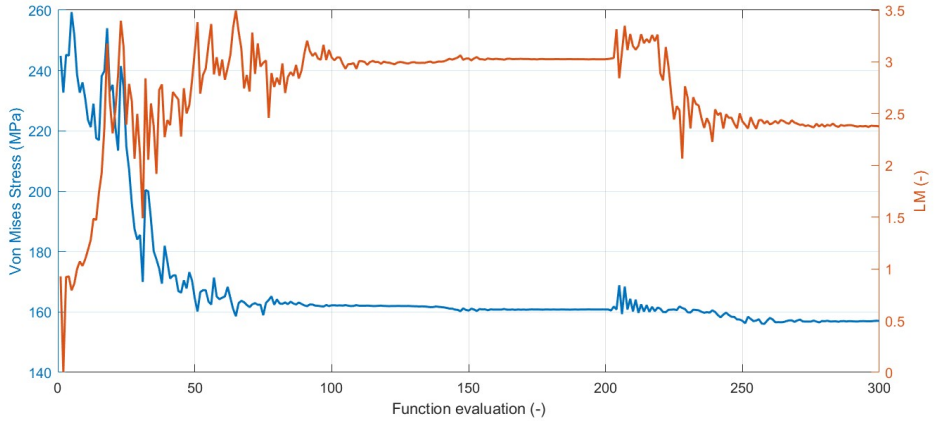

Figure 48: Second optimization results of structural Von Mises stress and Load multiplier.

As clearly illustrated in Figures 48 and 49, the integration of these elements has successfully led to a feasible design. The final thickness of main column group is evaluated to be around 6.4 centimeters, which corresponds to a significant decrease with respect to the previous value.

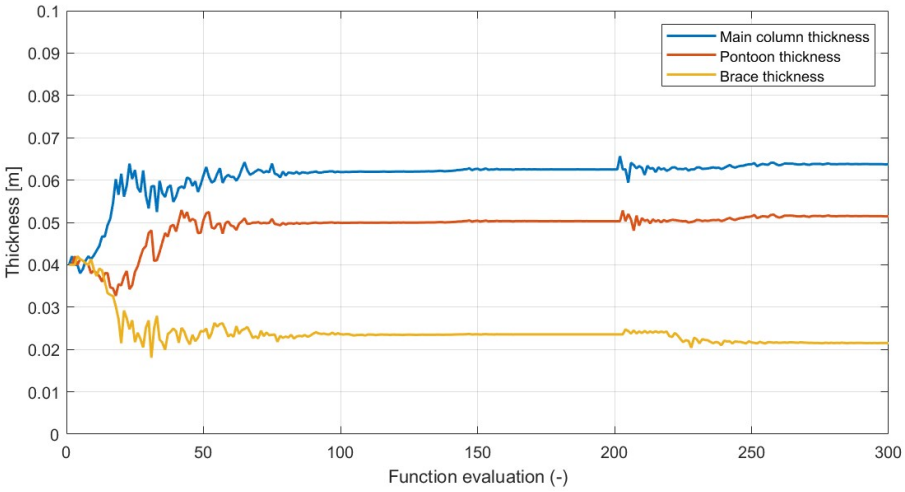

Figure 49: Second optimization results of thicknesses of surface elements.

Table 4 illustrates the values of important parameters in initial and final optimisations, which further justifies the importance of reinforcements to the structural performance of the platform.

	Initial optimisation	**Final otpimisation**
Steel mass	3925,4 tons	2927.19 tons
Equivalant Von Mises stress	149.47 MPa	157.03 MPa
Load multiplier	2.37	2.38
Man column thickness	12.7 cm	6.38 cm
Pontoon thickness	5.99 cm	5.15 cm
Brace thickness	5.52 cm	2.15 cm

Table 4: Comparison of optimisation results.

The stress distributions of final optimized structure are displayed in figure 50.

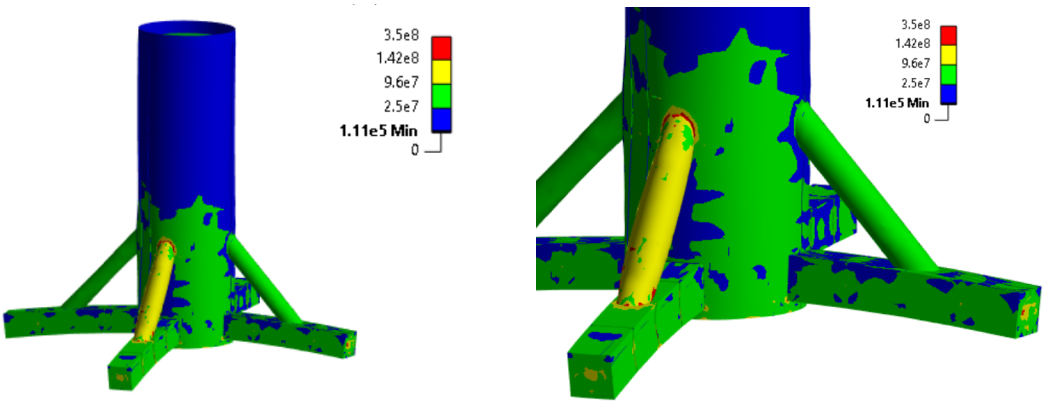

Figure 50: Final stress distribution at the end of the optimisation.

The stress is now primarily concentrated in the braces and at the junctions where the braces connect to the main column and the pontoons. The pontoon thickness is now 5 cm. Given these observations, there is potential for further optimisation of the pontoons, possibly by adding new stiffeners to these components.

Chapter 5

CONCLUSIONS AND FUTURE WORK

5.1 Conclusions

Wind energy demonstrates significant promise as a sustainable technology for generating power. Globally, onshore wind energy has already become a formidable player in the energy production sector. Transitioning to offshore wind energy offers substantial benefits and facilitates the utilization of additional areas for harnessing this resource. Several nations with shallow continental shelves, including Denmark, the Netherlands, Germany, and the United Kingdom, are already implementing offshore wind energy. Predominantly, these wind farms utilize fixed-bottom platforms and play a crucial role in the electrical generation of these countries.

The challenge of offshore exploration lies in the greater sea depths encountered in many areas, including Italy. Accessing these regions appears to be economically feasible primarily through floating platforms. The key issue

has been linking a structurally sound platform with cost-effectiveness. While some initiatives, like WindFloat and Hywind, have been put into practice, they continue to rely on substantial financial backing.
The previous chapters of this thesis have covered the structural optimization of a Tension Leg Platform (TLP) for Floating Offshore Wind Turbines (FOWTs); specifically, it has tackled some of the core design issues in platform design, contributing to overall FOWT performance improvement as well as cost and sustainability reduction. Incorporating hydrodynamic, aerodynamic, and static loadings into the structural analysis provided a realistic representation of operating conditions. A single-objective mass optimization algorithm that minimizes platform mass, subject to constraints on mechanical stress and buckling instability, was successfully employed.

One of the most important factors in the case study is that placing internal stiffeners to improve the structural integrity of a platform led to mass reductions. The designs that were then optimized showed that, if positioned in a clever way, stiffeners could save a lot of material without causing stability failures under operational loads. More-

over, the information on the trade-off between the design of platform geometry, load distribution, and material consumption can be useful for future FOWT layout.

5.2 Future Work

This research focused solely on the static aspect of the analysis where transient and dynamic aspects are overlooked. It is highly recommended to compare the results with time-domain simulations that adhere to standard design load cases, comprising of transient effects and wave loads.
Further studies can be carried out on the following aspects:

- Different shapes and placements of internal stiffeners can be explored.
- Different optimization algorithms can be used, and the results can be compared.
- Further study on the dependence of the location and number of internal stiffeners on the manufacturing costs is of particular interest.

BIBLIOGRAPHY

[1] International Energy Agency, “World Energy Outlook 2018 - EXECUTIVE SUMMARY,” 2018.

[2] U. S. Energy Information Administration, “Coal and the Environment - Energy Explained, Your Guide To Understanding Energy - Energy Information Administration.” [Online]. Available: https://www.eia.gov/energyexplained/index.php?page=coal_environment.

[3] International Energy Agency, "Nuclear Power", [Online]. Available: https://www.iea.org/energy-system/electricity/nuclear-power

[4] Let’s talk science, "Generating Electricity", [Online]. Available: https://letstalkscience.ca/educational-resources/backgrounders/generating-electricity-fossil-fuels

[5] U. S. Energy Information Administration, "Hydropower explained", [Online]. Available: https://www.eia.gov/energyexplained/hydropower/#:~:text=At%20hydropower%20plants%20water%20flows,applies%20pressure%20on%20a%20turbine

[6] Medium, "How is the electricity generated by a solar power plant distributed to consumers?" [Online]. Available: https://medium.com/@Breadarose/how-is-the-electricity-generated-by-a-solar-power-\plant-distributed-to-consumers-b684c3c304f3

[7] U. S. Department of Energy, "How does Solar work?", [Online]. Available: https://www.energy.gov/eere/solar/how-does-sol

ar-work#:~:text=When%20the%20sun%20shines%20onto,cell%2C%20causing%20electricity%20to%20flow

[8] U. S. Energy Information Administration, "Biomass explained", [Online]. Available: https://www.eia.gov/energyexplained/biomass/

[9] U. S. Department of Energy, "Geothermal basics", [Online]. Available: https://www.energy.gov/eere/geothermal/geothermal-basics#:~:text=Geothermal%20energy%20is%20heat%20energy,depths%20below%20the%20earth's%20surface

[10] The Energy Grid, "Geothermal Energy", [Online]. Available: https://theenergygrid.com/geothermal-energy/

[11] U. S. Department of Energy, "How Do Wind Turbines Work?", [Online]. Available: https://www.energy.gov/eere/wind/how-do-wind-turbines-work

[12] Greenmatch, "What Are the Advantages and Disadvantages of Renewable Energy?" [Online]. Available: https://www.greenmatch.co.uk/blog/2021/09/advantages-and-disadvantages-of-renewable-energy

[13] Ang,T.; Salem,M.; Kamarol,M.; Shekhar Das,H.; Alhuyi Nazari,M.; Prabaharan,N., "A comprehensive study of renewable energy sources: Classifications, challenges and suggestions", 2022.

[14] ENEL, "Wind Turbine", [Online]. Available: https://www.enelgreenpower.com/learning-hub/renewable-energies/wind-energy/wind-turbine

[15] IRENA, "Wind Energy", [Online]. Available: https://www.irena.org/Energy-Transition/Technology/Wind-energy#:~:text=The%20amount%20of%20power%20that,by%20a%20factor%20of%20eight

[16] Righter, Robert W. (2011). Windfall: wind energy in America today. Norman: University of Oklahoma Press.

[17] ScienceDirect, "Vertical Axis Wind Turbine", [Online]. Available: https://www.sciencedirect.com/topics/engineering/vertical-axis-wind-turbine

[18] CleanTechnica, "Vertical Axis Wind Turbines: Great In 1890, Also-rans In 2014", [Online]. Available: https://cleantechnica.com/2014/04/07/vertical-axis-wind-turbines-great-1890-also-rans-2014/

[19] cp.max ROTORTECHNIK, "Basic knowledge about rotor blades", [Online]. Available: https://www.cpmax.com/en/know-how-95/rotorwiki.html#:~:text=Rotor%20blades%20are%20one%20of,(2023)%20%5B1%5D

[20] Maciel, G. da S. G., "Desenvolvimento e Projeto Mecânico de uma Fundação para uma Turbina Eólica Offshore Engenharia Mecânica," 2017.

[21] Baghzouz, Y., "Characteristics of Wind Power Systems".

[22] Carlin, J., "Wind Turbine Blades 102".

[23] Kerrigan, S., "The Scientific Reason Why Wind Turbines Have 3 Blades," Interesting Engineering, 2018. [Online]. Available: https:

//interestingengineering.com/the-scientific-reason-why-wind-turbines-have3-blades

[24] "Wind Turbines: How Many Blades?," Danish Wind Industry Association, 2003. [Online]. Available: http://drÃÿmstÃÿrre.dk/wp-content/wind/miller/windpowerweb/en/tour/design/concepts.htm

[25] Aerotrope, "Riva Calzoni M33 Single Bladed Wind Turbine." [Online]. Available: https://www.aerotrope.com/what-we-do/wind/wind-turbine-design-case-studies/riva-calzoni.html.

[26] Milborrow, D., "Are three blades really better than two?," Windpower Monthly, 2011. [Online]. Available: https://www.windpowermonthly.com/article/1083653/three-blades-really-better-two.

[27] Wind farm BoP, "Gearbox in wind turbines", [Online]. Available: https://www.windfarmbop.com/gearbox-in-wind-turbines/

[28] Delony, J., "Foundation First: Designing Offshore Wind Turbine Substructures for Maximum Cost Reduction," Renewable Energy World, 2016. [Online]. Available: https://www.renewableenergyworld.com/articles/print/volume-19/issue10/features/wind/foundation-first-designing-offshore-wind-turbine-substructures-for-maximum-costreduction.html.

[29] Peyrard, C., "OFFSHORE WIND TURBINE FOUNDATIONS," 1989.

[30] A. Alsharedah, Y.; Newson,T.; El Naggar,M,H.; Black,J,A., "Lateral Ultimate Capacity of Monopile Foundations for Offshore Wind

Turbines: Effects of Monopile Geometry and Soil Stiffness Properties".

[31] ZOU,X.; Wang,Y.; Zhou,M.; Zhang,X., "Failure mechanism and combined bearing capacity of monopile–friction wheel hybrid foundation in sand-over-clay deposit".

[32] World Wind Technology, “Good foundations: the pros and cons of monopiles,” 2013. [Online]. Available: https://www.windpower-international.com/features/featuregood-foundations-the-pros-and-cons-ofmonopiles-4158694/

[33] Thomsen, K. (2014). Offshore wind: a comprehensive guide to successful offshore wind farm installation.

[34] BAM Nuttall Ltd, “Blyth Offshore Demontrator Wind Farm Project: First Gravity Base Foundation lowered onto sea bed,” 2017. [Online]. Available: https://www.bam.com/en/press/press-releases/2017/8/blythoffshore-demontrator-wind-farm-project-first-gravity-base.

[35] Buljan.A, "Mingyang Building Fish Farm-Equipped Offshore Wind Jacket Foundation", 2023.

[36] ISSMGE, [Online]. Available: https://www.issmge.org/publications/online-library

[37] Peyrard, C., “OFFSHORE WIND TURBINE FOUNDATIONS,” 1989.

[38] 4C Offshore, “Tripod Support Structures,” 2013. [Online]. Available: https://www.4coffshore.com/windfarms/tripod-support-structures-aid7.html

[39] EWEA, The next step for offshore wind energy, no. May. 2014.

[40] The Empire Engineering, "Guide to Offshore Wind Foundations".

[41] Rigzone, “How Do Spars Work?” [Online]. Available: https://www.rigzone.com/training/insight.asp?insight_id=307.

[42] The Empire Engineering, "Semi-Submersible, Spar and TLP – How to select floating wind foundation types?, [Online]. Available: https://www.empireengineering.co.uk/semi-submersible-spar-and-tlp-floating-wind-foundations/

[43] ScienceDirect, "Tension Leg Platforms", [Online]. Available: https://www.sciencedirect.com/topics/engineering/tension-leg-platforms

[44] Ghigo,A.; Niosi,F.; Paduano,B.; Bracco,G.; Matiazzo,G.; "MOORING SYSTEM DESIGN AND ANALYSIS FOR A FLOATING OFFSHORE WIND TURBINE IN PANTELLERIA", 2022.

[45] ANSYS, "What is Finite Element Analysis (FEA)?", [Online]. Available: https://www.ansys.com/simulation-topics/what-is-finite-element-analysis#:~:text=Finite%20element%20analysis%20(FEA)%20is,of%20the%20results%20FEM%20provides

[46] SimScale, “What is FEA | Finite Element Analysis?” [Online]. Available: https://www.simscale.com/docs/content/simwiki/fea/whatisfea.html

[47] ANSYS, "What is Finite Element Analysis (FEA)?", [Online]. Available: https://www.ansys.com/simulation-topics/what-is-finite-element-analysis#:~:text=Finite%20element%20an

alysis%20(FEA)%20is,of%20the%20results%20FEM%20provides

[48] IEA WIND, "Definition of the IEA Wind 15-Megawatt Offshore Reference Wind Turbine - Technical Report", 2020.

[49] Jonkman, J.; Butterfield, S.; Musial, W.; Scott, G., “Definition of a 5-MW Reference Wind Turbine for Offshore System Development,” 2009.

[50] Robertson, A. et al., “Definition of the Semisubmersible Floating System for Phase II of OC4,” 2014.

[51] Simões Da Silva, L. et al., Design of Joints in Steel and Composite Structures, 2nd ed. European Convention for Constructional Steelwork, 2016.

[52] NREL, "OpenFAST", [Online]. Available: https://www.nrel.gov/wind/nwtc/openfast.html

[53] Maciel, G. da S. G., “Desenvolvimento e Projeto Mecânico de uma Fundação para uma Turbina Eólica Offshore Engenharia Mecânica,” 2017.

[54] Platt, A.; Jonkman, B.; Jonkman, J., “InflowWind User’s Guide,” 2016.

[55] Jonkman, J. M.; Hayman, G. J.; Jonkman, B. J.; Damiani, R. R., “AeroDyn v15 User’s Guide and Theory Manual,” 2015.

[56] Jonkman, J. M.; Robertson, A. N.; Hayman, G. J., “HydroDyn User’s Guide and Theory Manual.”

[57] Hall, M., “MoorDyn User’s Guide,” 2017.

[58] Jonkman, J. M., “Dynamics Modeling and Loads Analysis of an Offshore Floating Wind Turbine,” 2007.

[59] Maciel, G. da S. G., “Desenvolvimento e Projeto Mecânico de uma Fundação para uma Turbina Eólica Offshore Engenharia Mecânica,” 2017.

[60] Jonkman, J. M.; Robertson, A. N.; Hayman, G. J., “HydroDyn User’s Guide and Theory Manual.”

[61] Sirigu,M.; Ghigo,A.; Giorgi,G.; Bracco,G., "A novel optimisation process for static structural finite element analysis of offshore wind turbine floating foundations ". In ISOPE International Ocean and Polar Engineering Conference (pp. ISOPE-I). ISOPE.

[62] Jonkman, J. M.; Robertson, A. N.; Hayman, G. J., “HydroDyn User’s Guide and Theory Manual.”

[63] Let’s talk science, "Generating Electricity: Nuclear Energy", [Online]. Available: https://letstalkscience.ca/educational-resources/stem-explained/generating-electricity-nuclear-energy

[64] U. S. Energy Information Administration, "Hydropower explained", [Online]. Available: https://www.eia.gov/energyexplained/hydropower/#:~:text=At%20hydropower%20plants%20water%20flows,applies%20pressure%20on%20a%20turbine

[65] YOKOGAWA, "Wind Power", [Online]. Available: https://www.yokogawa.com/it/industries/renewable-energy/wind-power/#Sfide

[66] U. S. Department of Energy, “The Inside of a Wind Turbine | Department of Energy.” [Online]. Available: https://www.energy.gov/eere/wind/inside-wind-turbine-0.

[67] De Vries, E., “How to service and maintain a wind turbine blade,” Windpower Monthly, 2012.

[68] Ge Vernova, "3 MW onshore wind turbine platform", [Online]. Available: https://www.gevernova.com/wind-power/onshore-wind/3mw-platform

[69] https://in.pinterest.com/pin/732538695651118668/

[70] CBM Connect, "Yaw Bearing System Fault Detected", [Online]. Available: https://www.cbmconnect.com/yaw-bearing-system-fault-detected/

[71] Meng Zhang,Bing Liu,Chongqi Gao, Md Nayim Hossain, Guifeng Zhao, "Wind-Induced Response Analysis and Fatigue Reliability Study of a Steel–Concrete Composite Wind Turbine Tower".

[72] Diogo Filipe da Silva Vasconcelos, "Structural Analysis of a Floating Foundation for Offshore Wind Power under Service Conditions".

[73] Autodesk, “Finite element analysis software (FEA software).” [Online]. Available: https://www.autodesk.com/solutions/simulation/finite-element-analysis.

[74] Park, Sungjun, and Joonmo Choung. 2023. “Structural Design of the Substructure of a 10 MW Floating Offshore Wind Turbine System Using Dominant Load Parameters.” Journal of Marine Science and Engineering.

[75] Global Wind Atlas, "Global Wind Atlas," [Online]. Available: https://globalwindatlas.info/.

“Fmin Function.” 2024. 2024. https://docs.scipy.org/doc/scipy/reference/generated/scipy.optimize.fmin.html.

“OpenFAST.” 2024. 2024. https://openfast.readthedocs.io/en/dev/source/user/general.html.

“Salome 9.9.0.” 2024 https://www.salome-platform.org/